

1 **Observation and modeling of the evolution of Texas power** 2 **plant plumes**

3
4 **W. Zhou¹, D. S. Cohan¹, R. W. Pinder², J. A. Neuman^{3, 4}, J. S. Holloway^{3, 4}, J.**
5 **Peischl^{3, 4}, T. B. Ryerson³, J. B. Nowak^{3,4}, F. Flocke⁵, W. G. Zheng⁵**

6 [1]{Department of Civil and Environmental Engineering, Rice University, Houston, Texas}

7 [2]{Office of Research and Development, US Environmental Protection Agency, North Carolina,
8 USA}

9 [3]{Chemical Sciences Division, Earth System Research Laboratory, NOAA, Boulder, Colorado,
10 USA}

11 [4]{Cooperative Institute for Research in Environmental Sciences, University of Colorado,
12 Boulder, Colorado, USA}

13 [5]{National Center for Atmospheric Research, Boulder, Colorado, USA}

14 Correspondence to: W. Zhou (zhouwei@rice.edu)

15 16 **Abstract**

17 During the second Texas Air Quality Study 2006 (TexAQS II), a full range of pollutants was
18 measured by aircraft in eastern Texas during successive transects of power plant plumes (PPPs).

19 A regional photochemical model is applied to simulate the physical and chemical evolution of
20 the plumes. The observations reveal that SO₂ and NO_y were rapidly removed from PPPs on a
21 cloudy day but not on the cloud-free days, indicating efficient aqueous processing of these
22 compounds in clouds. The model reasonably represents observed NO_x oxidation and PAN
23 formation in the plumes, but fails to capture the rapid loss of SO₂ (0.37 hour⁻¹) and NO_y (0.24
24 hour⁻¹) in some plumes on the cloudy day. Adjustments to the cloud liquid water content (QC)

1 and the default metal concentrations in the cloud module could explain some of the SO₂ loss.
2 However, NO_y in the model was insensitive to QC. These findings highlight cloud processing as
3 a major challenge to atmospheric models. Model-based estimates of ozone production efficiency
4 (OPE) in PPPs are 20-50% lower than observation-based estimates. Possible explanations for
5 this discrepancy include the observed rapid NO_y loss which biases high some observation-based
6 OPE estimates, and the model's under-prediction of isoprene emissions.



7

8 **1 Introduction**

9 Power plants are the leading point source emitters of SO₂ and oxides of nitrogen
10 (NO_x=NO+NO₂) (EPA, 2009). The large amount of SO₂ and NO_x emitted from power plants
11 has been linked to a series of environmental issues, such as acid deposition, photochemical O₃
12 and particulate matter (Srivastava et al., 2004; Ryerson et al., 2001; Brock et al., 2003; Flues et
13 al., 2002). Various regulations and market-based policies have been implemented to reduce these
14 emissions, including the Acid Rain Program (EPA, 2005) and the NO_x State Implementation
15 Plan Call (NO_x SIP Call) (EPA, 2004) in the United States. Power plants are among the most
16 accurately measured emission sources in the U.S. national emission inventory due to direct
17 smoke stack measurements by Continuous Emission Monitoring Systems (CEMS). Good
18 agreement has been found in comparing power plant emissions reported by CEMS with airborne
19 measurements of power plant plumes (PPPs) (Frost et al., 2006) and with satellite measurements
20 of NO₂ (Kim et al., 2006).

21 The emissions, transport, and chemical evolution of pollutants from power plants have been
22 investigated by multiple observational and modeling methods (Ryerson et al., 1998; Neuman et
23 al., 2004; Godowitch et al., 2008; Frost et al., 2006; Kim et al., 2006; Sillman, 2000). Airborne

1 measurement of chemical composition and meteorological parameters in PPP transects have
2 been conducted in several field campaigns over North America (Trainer et al., 1995; Ryerson et
3 al., 1998; Springston et al., 2005; Neuman et al., 2009)

4 SO₂ freshly emitted from power plant stacks is quickly diluted and undergoes chemical
5 evolution during plume transport. Previous aircraft measurements in PPPs have revealed that
6 gas-phase SO₂ oxidation is the key pathway for the SO₂ removal and the particle growth in PPPs
7 in the absence of clouds (Brock et al., 2002, 2003; Springston et al., 2005). SO₂ can also readily
8 dissolve in cloud water and then convert to sulfate via aqueous reactions. Previous studies
9 indicate that SO₂ in anthropogenic plumes has relatively long lifetime (10 hours to a few days) in
10 the lower troposphere (Ryerson et al., 1998; Lee et al., 2011) and can undergo intercontinental
11 transport if lifted into the middle and upper troposphere by deep convection (Fiedler et al., 2009).

12 Numerical simulations suggest that cloud droplet cannot effectively remove SO₂ plume when
13 plume passes through or interactive with intensive clouds, which has been rarely evaluated with
14 the observational data (Crutzen and Lawrence, 2000; Kreidenweis et al., 1997).

15 Several previous field studies have investigated the chemical evolution and lifetime of NO_x,
16 ozone production efficiency, and the loss rate of reactive nitrogen in PPPs (Ryerson et al., 1998;
17 Springston et al., 2005; Neuman et al., 2009). Even though numerical models have been utilized
18 to simulate the plume chemistry and regional transport of PPPs (Frost et al., 2006; Zaveri et al.,
19 2010), detailed model evaluation of pollutant concentrations at plume transects has been rarely
20 done due to the scarcity of the comprehensive airborne measurement of plume pollutants. Some
21 studies have reported the rapid loss of NO_y and HNO₃ in PPPs (Neuman et al.,
22 2004; Nunnermacker et al., 2000), but others have not (Ryerson et al., 2003).





1 In eastern Texas, power plants have significant contribution to the **primary emission** and high
2 ozone concentration in the region. While the several airborne observations have been used to
3 characterize the emissions of power plants and investigated the ozone formation in PPPs, the
4 modeling of plume transport with 3-D photochemical models and chemical evolution and the
5 detailed evaluation of plume simulation with the high spatial and temporal airborne observations
6 are not available yet. In several flights during the summer 2006 Second Texas Air Quality Study
7 (TexAQS II) (Parrish et al., 2009a), a NOAA WP-3 aircraft performed successive downwind
8 transects of PPPs in eastern Texas. The instruments aboard the WP-3 measured a full range of
9 **chemical** species, aerosol, and meteorological parameters at high time resolution and spatial
10 resolution. This study utilizes the rich data source to examine whether a 3D photochemical
11 model with a fine spatial resolution but without subgrid plume treatment can effectively simulate
12 the chemical and physical evolution of PPPs as they disperse and transport downwind. We focus
13 on the evolution of sulfur, reactive nitrogen, and O₃ in the plumes.



14

15 **2 Airborne measurement**

16 TexAQS II was a comprehensive observational campaign in eastern Texas from August to
17 October, 2006, which aimed to improve scientific understanding of the sources and atmospheric
18 processes responsible for the formation and distribution of O₃ and aerosols in the region (Parrish
19 et al., 2009a). PPPs observed during TexAQS II originated from eastern Texas coal-fired power
20 plants with a large range of reported NO_x and SO₂ emission rates (Table 1 and Fig. 1).

21 The measurements and operational characteristics of the NOAA WP-3 have been summarized
22 elsewhere (Parrish et al., 2009a). Instruments aboard the WP-3 measured numerous reactive
23 nitrogen species (NO, NO₂, HNO₃, NO₃, N₂O₅, PAN, peroxy propionyl nitrate (PPN),

1 methacrylol peroxy nitrate (MPAN), isoprene, CO₂, CO, SO₂, HCHO, major aerosol parameters,
2 UV-VIS actinic flux, relative humidity, and temperature (Tables A1a and A1b of Parrish et al.
3 (2009a) and the references therein). The instruments used in measuring major gas-phase species
4 (O₃, CO, CO₂, SO₂, NO, NO₂, HNO₃, NO_y, PAN, and isoprene) are summarized in Table S2 (in
5 supplementary materials). The time resolution of most instruments was 1 second, equal to
6 approximately 100m spatial resolution at typical WP-3 flying speeds.

7 Coal-fired power plants are major sources of SO₂ and NO_x, so their plumes can be identified
8 by elevated concentrations of SO₂ and NO_y (Ryerson et al., 1998; Ryerson et al., 2003). SO₂
9 enhancement can be a more reliable diagnostic of PPPs than NO_y since there are numerous
10 sources of NO_x, but coal-fired power plants are dominant sources of SO₂ in eastern Texas
11 (Ryerson et al., 2003; Neuman et al., 2009). Background SO₂ levels were consistently below 1
12 ppb, so this level of SO₂ is chosen as a threshold value for identifying PPPs.

13 In rural areas of northeastern Texas, power plants are also leading sources of CO and
14 anthropogenic CO₂ (Nicks et al., 2003), even though CO is not elevated in all PPPs. Airborne
15 measurements in 2000 and 2006 showed that CO and CO₂ could be signatures of the Martin
16 Lake, Monticello, and Welsh plumes, the concentration enhancements of which completely
17 overlap SO₂ and NO_y concentration enhancements at transects (Nicks et al., 2003). As the
18 atmospheric lifetime of CO₂ is years, it is a conservative species in plumes. CO has a lifetime of
19 one to two months in the atmosphere (Akimoto, 2003), thus serving as another conservative
20 species in PPPs. CO emissions from Martin Lake, Monticello, and Big Brown, which were
21 significantly underestimated in a previous emission inventory (1999), have been improved as
22 indicated by the observed CO/CO₂ in TexAQS II (Peischl et al., 2010).

1 Of the 18 WP-3 flights during TexAQS II, the 16 September and 25 September flights
2 measured successive cross-wind transects of PPPs from multiple power plants and the 19
3 September flight measured the Parish plume (Fig. 1 and Table S3). The 16 September flight
4 (11:00 to 15:00 local time) observed transects of plumes from the Martin Lake, Pirkey,
5 Monticello, and Welsh power plants at successive downwind distances (Fig. 2a). Since the three
6 plumes transported northward through rural areas devoid of other large anthropogenic SO₂
7 sources, SO₂ concentration enhancements clearly denote plume locations (Fig. 2a). Pirkey is
8 located just several km north-northeast (downwind) of Martin Lake, so their plumes cannot be
9 distinguished on this flight after the first Martin Lake transect; we refer to the plume as Martin
10 Lake (Ma-1) for simplicity. On 19 September, the WP-3 measured five plume transects of Parish
11 in Houston-Galveston Brazoria (HGB) metropolitan region. On 25 September (13:00 to 16:00
12 local time), the WP-3 measured two plume transects of Big Brown and Limestone under
13 northerly flow, and two plume transects of Parish in HGB (Fig. S5-S6 in supplementary
14 materials). All transects on the three days occurred at altitudes of 600-700 m, well within the
15 planetary boundary layer height of approximately 1500 m determined from measured
16 temperature profiles. The exception was five transects (Ma-4 to Ma-8) of the Martin Lake plume
17 at different heights but at the same downwind distance on 16 September.

18

19 **3 Model setup and input parameters**

20 Atmospheric chemistry for the episode was simulated by the Community Multiscale Air
21 Quality (CMAQ) model (Byun and Schere, 2006) version 4.7 (Foley et al., 2010), using the
22 CB05 chemical mechanism (Yarwood et al., 2005). Inline processing was applied to generate the
23 meteorology dependent emissions properties (i.e., biogenic emissions) (Foley et al., 2010). After

1 accounting for plume rise, most of the power plant emissions were modeled to be released
2 between 200 and 600 m elevation (Fig. S7).

3 The model was configured with 34 vertical layers and three one-way nested domains. The
4 outer two domains cover the continental U.S. (148×112 with 36 km grid resolution) and the
5 eastern U.S (279×240 with 12km grid resolution) including all of Texas, respectively. The
6 rectangular frame in Fig. 1 shows the fine domain with 4km grid resolution. A full description of
7 the modeling configuration and performance for the 12km domain can be found in Appel et al.
8 (2009). The CMAQ modeling for the 4km domain was from September 1-25, 2006, which
9 covers the days with WP-3 plume measurements.

10 Meteorology for the episode was simulated by the Fifth-Generation NCAR/Penn State
11 Mesoscale Model (MM5) (Grell et al., 1994) version 3.7.4 for the 36 km domain. For the inner
12 domains (12km and 4km modeling domains), the Weather Research and Forecasting Model
13 (WRF) version 3.0 (Skamarock et al., 2008) has lower biases in simulated wind and temperature
14 than MM5, so it was used for these domains. Thus, the meteorological field simulated by WRF
15 has been used to drive the air quality model. Both models had 34 vertical layers extending from
16 the surface up to 100 hPa. WRF was applied with Asymmetric Convective Model 2 PBL model
17 (Pleim, 2007), Pleim-Xiu Land Surface Model (Xiu and Pleim, 2001), Dudhia shortwave
18 radiation scheme (Dudhia, 1989), RRTM longwave radiation scheme (Mlawer et al., 1997),
19 Kain-Fritsch 2 subgrid convective scheme (Kain, 2004), and the Thompson microphysics
20 scheme (Thompson et al., 2004). MM5 used similar physical schemes. The consistency between
21 MM5 and WRF for the modeling domains was tested and verified (Appel et al., 2009).
22 Meteorological fields were converted to CMAQ-ready format by MCIP version 3.4.2 (Otte and
23 Pleim, 2009).

1 Emission inputs for the three modeling domains were generated by Sparse Matrix Operator
2 Kernel Emissions (SMOKE) (EPA, 2006) based on the National Emission Inventory for 2005.
3 Mobile emissions were projected to 2006 and actual CEMS data were used for point sources.
4 BEIS3.12 (Environmental Protection Agency Biogenic Emissions Inventory System 3.12)
5 (<http://www.epa.gov/asmdnerl/biogen.html>) was applied to compute the biogenic emissions.

6 NO_y species in the CB05 chemical mechanism are NO, NO_2 , NO_3 , N_2O_5 , HONO, HNO_3 ,
7 PNA (peroxynitric acid), PAN (peroxyacetyl nitrate), PANX (C3 and higher peroxyacyl
8 nitrates), and NTR (organic nitrate). The sum of all these species (with $\text{N}_2\text{O}_5 \cdot 2$) is the
9 concentration of NO_y from the model. CMAQ simulates CO but not CO_2 .

10 To identify and analyze the impact of each power plant, a zero-out simulation is run with the
11 emissions of that facility removed from the base emission inventory. The difference between
12 concentrations in the base simulation and each zero-out simulation represents the zero-out-
13 contribution (ZOC) of that power plant, which indicates the overall effect due to its emission and
14 is not influenced by the nonlinear feature of plume chemistry. One base simulation and five zero-
15 out simulations for the five power plants were performed. We focus our analyses on SO_2 and
16 NO_y species, whose concentration are greatly elevated in PPPs.

17 The aqueous processing module in CMAQ (Walcek and Taylor, 1986) processes the
18 absorption of gas-phase species and accumulation-mode aerosols separately. The gas-phase
19 absorption into liquid water content of clouds depends on the thermodynamic equilibrium,

20 whereas accumulation-mode aerosols are considered to be absorbed completely into the cloud
21 water. The dissociation of compounds into ions, oxidation of S(IV) to S(VI) by aqueous H_2O_2 ,
22 O_3 , Fe(III) and Mn(II) etc, and wet deposition are also processed in the model. For
23 computational efficiency, CMAQ does not transport cloud-aqueous concentrations separately

1 from gas-phase concentrations between model grids. At the end of the cloud processing module,
2 the cloud concentrations are removed and the mass of each species is passed to either gas-phase
3 or aerosol concentrations.

4 In this study, the advection schemes used in the processing pollutant transport by the CMAQ
5 model are Piecewise Parabolic Method (PPM) (Colella and Woodward, 1984) and Yamartino-
6 Blackman Cubic Scheme (YAM) (Yamartino, 1993). The Asymmetric Convective Model
7 version 2 (ACM2) (Pleim, 2007) was used to simulate the vertical mixing of pollutants in
8 CMAQ.

9

10 **4 Results and Discussion**

11 During airborne measurement on the three days, ground temperature was 24.4-35.5°C
12 (average: 29.0 °C) and surface wind was 0-7.2 m/s (average: 3.1m/s) at ground-based monitors
13 in eastern Texas. At 600-700m (WP-3 typical flying height), the observed ambient temperature
14 was 23.7-30.3°C (average: 26.8 °C), wind speed was 1.6-12.0 m/s (average: 6.4 m/s) and no
15 precipitation was observed. The height of the planetary boundary layer (PBL), determined from
16 the vertical profiles of equivalent potential temperature for the three days, was about 1500 m on
17 16 September and about 1000 m in the HGB region on 19 and 25 September.

18 The CEMS-reported SO₂ and NO_x emissions of big power plants in the eastern U.S. were
19 previously evaluated based on with WP-3 measurements of PPPs in 2004 (Frost et al., 2006).
20 Since the emitted NO_x in PPPs can quickly be oxidized to NO_z (NO_z = NO_y-NO_x), the observed
21 enhancements of NO_y and SO₂ serve as the basis for evaluation. The strong correlation between
22 NO_y and SO₂ for all first plume transects (R²=0.68~0.98) suggests that the power plants were the

1 dominant sources of these gases there. The three ratios of these plants show strong consistency
2 within the uncertainties of the measurements, although the model slightly under-predicts
3 SO_2/NO_y ratios (Table 2). Likewise, previous studies have reported strong consistency between
4 CEMS(SO_2/NO_x) and OBS(SO_2/NO_y) (Frost et al., 2006; Ryerson et al., 2003; Ryerson et al.,
5 2001).

6 **4.1 Evaluation of plume dispersion and transport**

7 On 16 September, the WP-3 observed mostly southerly winds with average wind speeds of
8 6.9 m/s. The southerly winds allowed PPPs of Monticello and Welsh to remain distinct in both
9 model and observation (Fig. 2) but caused the Martin Lake and Pirkey plumes to coincide since
10 the two plants are just 18.5 km apart. Maximal SO_2 enhancements for each plume transect were
11 used to identify the plume centers in observations and modeling results to enable comparative
12 analyses of observations and modeling results. The plumes produced by CMAQ mostly have
13 similar spatial extent to the measured plumes on 16 September (Fig. 2), 19 and 25 September
14 (Fig. S5-S6). The wind speed and direction in the model were more homogeneous than observed
15 winds, resulting in slight differences between modeled and observed locations of the plumes and
16 plume centers (Fig. 2).

17 The high-resolution aircraft observations were compared with the model outputs extracted
18 from the corresponding grid cells, adjusted to align the modeled and measured plume peak
19 locations as necessary. Since the aircraft was flying consistently at approximately 100 m/s at
20 each plume transect, each gridline interval in Fig. 3 (40 seconds) is equal to the spatial distance
21 of 4 km (one grid cell).

1 The 16 September flight path proceeded northward in 14 successive crosswind (east-west)
2 transects, the first 12 of which intercepted the Martin Lake (and Pirkey) plumes (Ma-1 to Ma-12
3 in Fig. 2; Ma-4 to Ma-8 are increasing altitudes at the same transect) and the last four of which
4 intercepted the Monticello and Welsh plumes (Fig. 2). The extensive observation of the Martin
5 Lake plume provides a unique opportunity to examine plume evolution from the emission stack
6 until dilution to background levels. Comparisons between modeled and observed SO₂, NO_y, and
7 CO mixing ratios are shown for each successive plume transect of the two days in Fig. S1-S4.

8 At the first transect of the Martin Lake, Monticello, and Welsh plumes, the model generates
9 lower peak SO₂ and NO_y concentrations and wider plumes than was observed. This likely
10 reflects the inability of the 4-km resolution model to resolve subgrid-scale plume structure in the
11 initial formation of a plume. No subgrid or Plume-in-Grid (PinG) was used in the modeling.

12 The modeled CO captured the observed extent at each plume transect, slightly under-
13 estimating the peak values (Fig. 3). The modeled SO₂ (18ppb) at Ma-2 matched the observed
14 peak (23 ppb) closely as subgrid effect weakened and the plume width was larger than one grid
15 cell. As the plume transported to Ma-3, the modeled SO₂ (14ppb) was higher than the observed
16 peak (7ppb). The modeled SO₂ at plume center was consistently higher than the observed while
17 the background SO₂ matched observations.

18 The measured CO at the plume center declined only from 240 (Ma-1) to 150 ppb (Ma-3).
19 However, SO₂ was observed to decline by more than a factor of 10 from Ma-1 to Ma-3,
20 indicating rapid loss.

21 Ma-4 through Ma-8 observed the Martin Lake plume at the same downwind distance (53 km)
22 but flew at different altitudes (Ma-4 to Ma-8 of Fig. S1; Table S3). SO₂ emission from Martin
23 Lake was modeled to occur mostly at 400 m, accounting for the stack height and plume rise (Fig.

1 S7). At 1800 m (Ma-4), which was near the top of the PBL, no enhancement of SO₂, NO_y, or
2 CO was simulated but a weak SO₂ plume was observed, implying that the model failed to
3 capture some of the observed upward transport. At lower flight altitudes (between 660 and 300
4 m, corresponding Ma-6 to Ma-8 in Fig. S1), the model effectively simulated plume extent. The
5 comparisons between the modeled and observed SO₂, CO and NO_y species on 19 and 25
6 September are shown in Fig.S1-S4.

7 **4.2 Correlations between conservative and non-conservative species**

8 In this section, we explore the correlation between conservative and non-conservative species
9 from the observed plume concentrations. The correlations are presented by the slopes and R² of
10 the least-square-fit between conservative and non-conservative species. At the time scale of PPP
11 transport (a few hours), CO and CO₂ are expected to experience similar dispersion and minimal
12 loss to chemistry or deposition, leading to near constant slopes of CO to CO₂. CO and CO₂
13 concentrations were strongly correlated within the Martin Lake and Monticello plumes and the
14 slopes of CO to CO₂ held steady as both plume aged (Fig. 4) (for Ma-1 to Ma-3 and Ma-6 to
15 Ma-12, slopes of the least square fit: 0.58~0.71 ppb/ppm, R²: 0.89~0.96; for Mo-1 to Mo-4,
16 slopes of the least square fit: 4.3~5.3 ppb/ppm, R²:0.77~0.94), indicating the same extent of
17 dispersion exerting on the concentration evolution of CO and CO₂. For the Welsh and Big
18 Brown plumes, only the first one or two transects had the strong correlation between CO and
19 CO₂, with their later transects likely affected by nearby CO or CO₂ emissions. Due to the strong
20 interference from HGB urban emissions of CO, no clear correlation between CO and CO₂ could
21 be found in the Parish plume.

1 Concentrations of SO₂ and reactive nitrogen species in PPPs are strongly affected by
2 chemical reactions, heterogeneous conversion, deposition, dispersion, and cloud processing.
3 Dispersion is expected to have the same extent of impact on both conservative (e.g., CO₂ and
4 CO) and non-conservative species (e.g., SO₂, NO_x, HNO₃, and PAN). Thus, the variations of
5 slopes between non-conservative and conservative species reflect the impact of plume chemistry,
6 deposition and heterogeneous processing on non-conservative species.

7 Given that the observed SO₂ and CO₂ in all plumes showed strong correlations, CO₂ could
8 serve well as a signature of PPPs. However, since CO₂ is not modeled by CMAQ, CO is selected
9 as the conservative species for the purpose of comparison between the model and the
10 observations. CO is a signature emission of some but not all power plants in Texas. In observed
11 PPPs, only in the Martin Lake and Monticello plumes could the strong correlations between the
12 non-conservative species (SO₂, reactive nitrogen species) and CO be found at all transects. In the
13 first one or two transects of the Big Brown and Welsh plumes, SO₂ strongly correlates with CO.

14 **4.3 Evaluation of SO₂ plume evolution**

15 On 19 September, under the clear-sky background (Fig. S9), the normalized SO₂ to CO ratio
16 from the model and the normalized SO₂ to CO₂ ratio from the observation matched closely for
17 the Parish plume, both of which shows the slow SO₂ loss (Fig. 8). At the plume age of 11 hours,
18 only 25% SO₂ was removed in both the modeling and the observation. Thus, the model can
19 capture SO₂ evolution when no cloud processing occurs.

20 However, plume observations demonstrate rapid loss of SO₂ in the 16 September plumes
21 (Martin Lake, Monticello and Welsh) (Fig. 5). For the Martin Lake transects, the decreasing
22 trend of SO₂/CO fits to an exponential function with a first-order loss rate of 0.38 hour⁻¹, the

1 inverse of which is a lifetime of 2.6 hours ($R^2=0.94$) (Fig. 5). SO_2/CO from the model decreases
2 far slower as plume ages with a loss rate of 0.016 hour^{-1} (lifetime of 62.5 hours), which suggests
3 the model significantly underestimates SO_2 loss for the Martin Lake plume. Similarly, for the
4 Monticello plume, the curve fit of observed SO_2/CO indicates an SO_2 lifetime of 2.7 hours (loss
5 rate of 0.37 hour^{-1}) compared to a modeled SO_2 lifetime of 17.2 hours. Although SO_2 and CO
6 were not strongly correlated in observations of the other plumes, diminishing SO_2/CO_2 ratios
7 indicate that rapid SO_2 loss also occurred in the Welsh plume, but not in the Big Brown and
8 Parish plumes during cloud-free days (Fig. 5 and 8).

9 The lifetime of SO_2 against gas-phase oxidation by OH is a few days to one week, and SO_2
10 lifetime against dry deposition approximates one day in the boundary layer. Thus, gas-phase
11 oxidation and dry deposition are insufficient to explain the rapid loss of SO_2 in the 16 September
12 plumes. The observed rapid loss of SO_2 in the 16 September plumes may indicate aqueous-
13 processing by the scattered clouds that were presented on this day. In clouds, SO_2 can be
14 substantially dissolved in water droplets and subsequently be oxidized to form H_2SO_4 in cloud
15 water far more rapidly than the gas-phase process.

16 Observational data indicates scattered cloudiness on 16 September and clear skies on 19 and
17 25 September. MODIS images of cloud and aerosol optical depth
18 (http://ladsweb.nascom.nasa.gov/browse_images/) show that there were scattered clouds over
19 eastern Texas on 16 September and it was a clear-sky and sunny day on 19 and 25 September.
20 On 16 September, the measured photolysis rates of NO_2 and NO_3 oscillated by a factor of 2
21 during the aircraft measurement, in contrast to less variability on 19 and 25 September (Fig. S8).
22 The cloudy meteorological condition on 16 September, indicated by the variations of photolysis
23 rates, agrees with scattered clouds captured by the satellite cloud image (Fig. S9). The relative

1 humidity measured from Ma-4 to Ma-8, when the WP-3 descended from 1800 to 300 m at the
2 same downwind distance of Martin Lake, reached saturation between 1800~1000 m, implying
3 clouds distributed at that altitude and potentially interacting with the plume (Ma-4 and Ma-5 in
4 Fig. S1).

5 The model successfully simulated the distribution of scattered clouds over northeastern Texas
6 on 16 September indicated by a MODIS cloud image (Fig. S9 and S10), but placed them
7 predominately between 2500 and 4000 m altitude as indicated by the cloud bottom height
8 (CLDB) in the model (Fig. S10), well above the PPPs which resided under the PBL (~1000-1500
9 m) as shown in the vertical distribution of plume SO₂ for Martin Lake, Monticello, and Welsh
10 plumes (Fig. S11-S12). The liquid water mixing ratio (QC) from the layer 10 and above in the
11 model was zero. Thus, no significant cloud processing was modeled to occur in the base
12 modeling, so the observed rapid loss of SO₂ in the 16 September plumes could not be replicated.

13 Could CMAQ have simulated the rapid SO₂ loss on 16 September if the meteorological
14 model had placed the clouds at lower altitudes in contact with the PPPs? The cloud module in
15 CMAQ includes two mechanisms for removing pollutants: aqueous chemical reactions and
16 scavenging and wet deposition. SO₂ absorption into cloud droplets and subsequent oxidation are
17 explicitly represented. The absorption is governed by the thermodynamic equilibrium. The
18 aqueous S(IV) is then oxidized to S(VI) by H₂O₂, O₃, metal ions (Fe(III) and Mn(II)), and
19 methylhydroperoxide (MHP), and peroxyacetic acid (PAA). Since no precipitation was observed
20 during the airborne measurements, pollutants were not expected to be scavenged.

21 Cloud parameters of meteorological inputs are perturbed to diagnose how efficiently
22 pollutants such as SO₂ and NO_y are removed from plumes. Specifically, the cloud bottom height
23 in the meteorological field on 16 September is adjusted to 1000 meters so that the plumes

1 interact with clouds during their transport. Liquid water content QC is the cloud parameter
2 determining the extent of the pollutant aqueous processing. The cloud aqueous module can be
3 executed only if QC is larger than 0.01 g/kg. Initially, QC over northeastern Texas in the base
4 model is zero and the maximum QC over the entire domain is about 0.4 g/kg. In the perturbation
5 cases, we uniformly increase QC to the levels from modest to strong cloudy conditions (from
6 700 m to 1000 m over northeastern Texas, see Fig. S13). In the first perturbation case (denoted
7 QC_0.05), QC is set to 0.05 g/kg $\approx 0.05 \text{ g/m}^3$, equivalent to fog, a modest cloud). Then QC is
8 increased to 0.5 g/kg $\approx 0.5 \text{ g/m}^3$, equivalent to stratocumulus clouds) and 5 g/kg $\approx 5 \text{ g/m}^3$,
9 equivalent to cumulonimbus clouds), respectively, representing extremely cloudy conditions.

10 In the base modeling for the Martin Lake plume, only 11% SO₂ is removed in the model (the
11 normalized SO₂/CO decreased to 0.89 from Ma-1 to Ma-12). In the QC_0.05 case, 25% of SO₂
12 is removed during that span (SO₂/CO decreases from 0.344 (Ma-1) to 0.257 (Ma-12)), far short
13 of the observed 92% SO₂ removal (SO₂/CO decreased from 0.480 (Ma-1) to 0.041 (Ma-12) in
14 observations) (Fig. 5). The cloudier scenarios yield 66% (QC=0.5 g/kg) and 81% (QC=5.0 g/kg)
15 SO₂ removal, still below the observed rate.

16 Four S(IV) oxidation reactions are explicitly implemented in the cloud aqueous module, i.e.
17 H₂O₂, O₃, metal (Fe(III) and Mn(II)), MHP, and PAA oxidations. In QC_0.05, S(IV) oxidation
18 is dominated by H₂O₂ oxidation, with 96.2% of S(IV) oxidation occurring by H₂O₂ in the
19 Martin Lake plume. Only about 1.7% of S(IV) oxidation was by the metal ions.

20 In the default CMAQ cloud module, Fe(III) and Mn(II) are uniformly set to 0.01 and 0.005
21 $\mu\text{g/m}^3$ over the domain. These values are assumed to represent the aqueous metal ion
22 concentrations in the background atmosphere. However, power plants are major emission
23 sources of particulate metals (Alexander et al., 2009). Fe(III) and Mn(II) in the power plant

1 plumes are expected to be higher than the background levels, thus potentially enhancing the
2 aqueous oxidation of sulfur in PPPs. In another perturbation case, both Fe(III) and Mn(II)
3 concentrations are increased by a factor of 10 with QC setting to 0.05 g/kg (called QC_METAL
4 hereafter). The increase of Fe(III) and Mn(II) is within the range of metal ion concentrations
5 measured in fogs and cloud water (Raja et al., 2005;Parazols et al., 2006). SO₂ removal in
6 QC_METAL was more rapid than that of QC_0.05 (Fig. 5). At the last plume transect, SO₂
7 decreased by 33%, compared to the 25 % SO₂ removal in QC_0.05, suggesting the increased
8 metals in plume lead to more SO₂ removed in cloud water. Thus, some combination of
9 enhancements in cloud liquid water content and metals concentrations may help explain the
10 observed rapid SO₂ loss rates in the cloudy day plumes.

11 Few studies have observed rapid SO₂ loss in anthropogenic plumes, though similar rates of
12 SO₂ loss have been found in volcanic plumes (Oppenheimer et al., 2010;Rodríguez et al., 2008).
13 These studies proposed that cloud aqueous processing is the mechanism for the rapid SO₂
14 removal. The comprehensive airborne measurement of plume concentrations and meteorological
15 parameters supported by satellite images in this study confirms that the cloud processing caused
16 the rapid SO₂ loss. SO₂ taken up by cloud droplet and subsequent aqueous oxidation, as a
17 complex process affected by QC, droplet pH, and the oxidant concentrations, and catalysis in the
18 droplets etc, are a major challenge to models. Earlier studies have also found that models can
19 underestimate SO₂ loss rates in clouds (Crutzen and Lawrence, 2000;Kreidenweis et al., 1997).

20 **4.4 Evaluation of plume chemistry of reactive nitrogen**

21 In PPPs, HNO₃, NO₃, N₂O₅, PAN, and other organic nitrates are formed via the NO_x
22 chemical reactions. Freshly emitted NO_x titrates O₃ and consumes OH, resulting in slow

1 formation of HNO₃ and no formation of PAN in the initial plume (Karamchandani et al., 1998).
2 As a plume dilutes, OH levels recover and HNO₃ and other products form from NO_x oxidation.
3 Previous daytime observations of PPPs concluded that HNO₃ and PAN were the major (more
4 than 90%) products of NO_x oxidation in PPPs (Neuman et al., 2006; Neuman et al., 2004;
5 Ryerson et al., 2003; Ryerson et al., 2001). The observational data in this study also show that
6 HNO₃ and PAN were the only two major oxidation products in PPPs, with NO₃ and N₂O₅ and
7 other organic nitrates at least one order of magnitude lower in plume transects.

8 The measured and modeled NO_x, HNO₃, and PAN are shown for comparison in Fig. S2 and
9 S3. NO_x was higher than HNO₃ until the plume transported 2.0 hours at Ma-7 and Ma-8. The
10 model generally captured the observed evolution of reactive nitrogen species NO_x, HNO₃, and
11 PAN in the plume, simulating the transition from NO_x to HNO₃ dominance and approximately
12 matching the observed PAN levels. However, the simulated HNO₃ concentrations were higher
13 than observed, implying over-prediction of HNO₃ formation or under-prediction of HNO₃ loss.


14 The oxidation of NO_x by radicals approximates as a first-order reaction if radical
15 concentrations are assumed to be constant in the plume. The observed NO_x/CO fits to an
16 exponential decay function (for Martin Lake, R²=0.85; for Monticello, R²=0.86; Fig. 6),
17 corresponding to NO_x lifetimes of 2.6 and 1.2 hours for the Martin Lake and Monticello plumes,
18 respectively. The NO_x lifetimes computed here are consistent with the NO_x lifetimes (1.0~1.6
19 hours) estimated for both plants in TexAQS 2000 (Neuman et al., 2004). The declining trends of
20 NO_x/CO from the model and the observation closely match in the Martin Lake and Monticello
21 plumes, with discrepancies only in the initial transects due to the inability of the model to resolve
22 subgrid-scale plume structure (Fig. 6).

1 The ratios of HNO_3/CO and PAN/CO are compared between the model and observations to
2 explore chemical evolution in the Martin Lake and Monticello plumes. We find that the model
3 captures the PAN formation very well, closely matching observed trends as the plumes age (Fig.
4 6 and Fig. S2). The modeled HNO_3/CO , however, was 0.7~6.6 times larger than observed. Given
5 the good agreement between the modeled and observed NO_x oxidation and PAN formation, the
6 HNO_3 gap between the model and the observation on the cloudy day implies that HNO_3 , while
7 being formed during plume transport, was rapidly removed from the atmosphere, which is not
8 captured by the model.

9 Unexpectedly rapid loss of NO_y has also been reported by some measurement studies of
10 biomass burning (Takegawa et al., 2003) and PPPs (Neuman et al., 2004), but not in others
11 (Ryerson et al., 2003). When NO_x is oxidized to other reactive nitrogen species, the reactive
12 nitrogen may be removed from the atmosphere via rain scavenging, dry deposition,
13 heterogeneous conversion to aerosol, and cloud processing, resulting in the loss of NO_y .
14 Assuming a first-order decline of NO_y/CO (Fig. 7), the observed NO_y loss rate was 0.15 hour^{-1}
15 for the Martin Lake plume whereas the modeled NO_y loss rate was lower by a factor of 6 (0.026
16 hour^{-1}). For the Monticello plume, the observed NO_y loss rate (0.24 hour^{-1}) was 2.3 times the
17 modeled. The observed NO_y/CO_2 in Martin Lake, Monticello, and Welsh plumes had the similar
18 extent of NO_y loss, especially during the early plume age (≤ 2 hours) when NO_y/CO declined by
19 40~50% (Fig. 7).

20 On 19 September, a cloud-free day, the model effectively simulates the observed slow
21 removal of NO_y (Fig 8). NO_y loss on the cloudy day likely reflects deposition of highly soluble
22 HNO_3 , since the other main NO_y constituents (NO_x and PAN) have low water solubility, cannot
23 directly convert to aerosol, and have negligible dry deposition in plume. NO_x oxidation and

1 thermal decomposition of PAN do not shift the gas-phase NO_y budget since their products are
2 also gas-phase NO_y constituents. The measured NO_3^- was minor in the inorganic aerosol
3 composition, indicating that the loss of HNO_3 to aerosol- NO_3^- was negligible under the high
4 ambient temperatures (the measured average temperature was 28.9°C) and the lack of ammonia
5 enhancement beyond levels needed to neutralize the sulfate in the PPPs (Nowak et al., 2010).
6 Given that no wet precipitation was reported on the flight days, no rain scavenging is expected to
7 have occurred. HNO_3 may have rapidly dissolved in cloud droplets if the plume interacted with a
8 cloud, as is possible under the 16 September scattered cloudiness conditions discussed earlier.

9 In contrast to the SO_2 results, the cloud perturbation scenarios did not significantly impact
10 modeled concentrations of NO_y species. Among NO_y species, HNO_3 is the only one to be
11 processed by the cloud module. Even raising QC to 5.0 g/kg, there is no scavenging removal of
12 HNO_3 since no wet deposition happens in the absence of precipitation. At the end of the cloud
13 module, the aqueous concentration of HNO_3 in cloud is passed to either gas-phase or aerosol
14 species. Also, the ratio HNO_3 to total NO_y is assumed to be constant. Thus, in the cloud aqueous
15 modeling, HNO_3 is expected to be insensitive to QC 

16 **4.5 Evaluation of O_3 simulation in PPPs**

17 Various numerical models have been applied to simulate the O_3 chemistry of PPPs (Sillman,
18 2000; Springston et al., 2005; Frost et al., 2006; Zaveri et al., 2010). The simulation of 3-D models
19 are as the most widely used tool to assess the effectiveness of emission controls of power plant
20 pollutants while the model performance has been merely examined with ground concentrations
21 (Mauzerall et al., 2005; Vijayaraghavan et al., 2009; Godowitch et al., 2008a; Godowitch et al.,
22 2008b). In this study, the simulated plume concentration and evolution which essentially happens

1 at several hundred meters above ground have been compared to those aircraft measurement at
2 plume transects. In this section, the O₃ concentration and OPE are compared with the observed
3 at each plume transect in detail. The model overestimated background O₃ by 8~15 ppb during
4 the flights (Table S4). Sensitivity modeling shows that boundary conditions were the biggest
5 contributor to background O₃ levels. Thus, we focus on the differences (ΔO_3) between plume
6 and background O₃ mixing ratios to assess model performance for O₃ formation from power
7 plant plumes (Table S4).

8 The model accurately simulates that the Monticello and Welsh plumes shift from being
9 depleted to being enriched in O₃ between transect 1 and 2, and predicts the transition to occur
10 one transect sooner than observed for Martin Lake. All of these plumes traversed rural regions of
11 northeastern Texas where biogenic isoprene is abundant. However, the model underestimates the
12 amount of O₃ enrichment downwind by 20-70% (Ma-9 to Ma-12, Mo-2 to Mo-4, We-2 to We-
13 4). The model also underestimates titration in the initial transects, reflecting the more rapid
14 dilution of NO_x in the model.

15 OPE illustrates the number of O₃ molecules formed per molecule of NO_x irreversibly
16 oxidized to NO_z species (Liu et al., 1987). Box and 2D Lagrangian models driven by the
17 observational data have previously computed OPE of pollution plumes and at ground-based
18 monitors (Sillman, 2000;Zaveri et al., 2003). Three dimensional global models have been applied
19 to calculate the global and regional OPE averaged at coarse scale (Fang et al., 2010;Hudman et
20 al., 2009). It is more relevant to apply the regional 3D model at fine resolution in deriving the
21 ozone sensitivities and OPE for regional and urban air quality strategies. OPE from 3D regional
22 models, however, has rarely been evaluated with the observation-based results at the plume-
23 transect scale due to the scarcity of measurements (Yu et al., 2010;Godowitch et al., 2008b). This

1 study computes the OPE at each plume transect from the model and then compares it with the
2 corresponding observational results. In the model, OPE is determined from the ratio ZOC_{O_3} to
3 ZOC_{NO_z} . The observation-based OPE is typically derived from the least square slope of O_3
4 versus NO_y - NO_x (NO_z) (Trainer et al., 1993; Kleinman et al., 2002; Griffin et al., 2004; Ryerson
5 et al., 2003).

6 For Martin Lake, Monticello, and Welsh, while O_3 production evolves from being depleted to
7 being formed, OPE exhibits a steady increase, consistent with OPE trends from PPPs in the
8 southeast U.S. (Ryerson et al., 2001) and in Texas in 2000 (Springston et al., 2005; Ryerson et al.,
9 2003). OPEs from Martin Lake (Ma-6), Monticello (Mo-4), and Welsh (We-4) plumes at similar
10 plume ages are compared in Fig. 9. OPEs for Monticello and Welsh were remarkably similar
11 (Fig. 9), reflecting approximately equal O_3 formation potentials of these facilities with similar
12 NO_x emission rates (Table 1). Martin Lake emitted about two times as much NO_x as Monticello
13 and Welsh, and thus exhibited a smaller OPE (7.25). OPE in the Big Brown plume (Bi-1) was
14 1.7 at a plume age of 1.3 hours, lower than the similar-plume-age OPE of Martin Lake (2.6, Ma-
15 3) and Welsh (4.6, We-2), but close to the OPE of Monticello (1.4, Mo-2). OPE could not be
16 quantified in the subsequent Big Brown transect due to lack of correlation between O_3 and NO_z .
17 The Parish plume exhibited an OPE of 4.4 at a plume age of just 0.6 hours, suggesting rapid O_3
18 formation under the influence of Houston region anthropogenic VOCs.

19 For the Martin Lake, Monticello, and Welsh plumes, the modeled OPEs steadily increase
20 from O_3 titration (negative OPE) to rapid O_3 formation, showing similar trends to the observed
21 OPEs. The modeled maximum OPEs are systematically about a factor of 2 lower than the
22 observed for these plumes likely due to the rapid loss of NO_y observed during the cloudy day
23 (Table S4). Since the definition of OPE implicitly assumes that NO_y is conservative in plumes,

1 the accuracy of the observation-based OPE may be undermined due to the rapid loss of NO_y in
2 this study.

3 It should also be noted that the model tended to under-predict measured isoprene
4 concentrations. Observed isoprene concentrations averaged over all transects, is higher than the
5 modeled average by 51.3%. We perturb domain-wide isoprene emission rates by this factor in
6 the model to investigate how much impact the isoprene discrepancy has on the O_3 formation in
7 plumes. After perturbation, the simulated ZOC_{O_3} has a maximum increase of 3 ppb (Ma^{-2}). The
8 maximum O_3 increase for Monticello and Welsh is 1.5 and 2 ppb, respectively. OPEs of Martin
9 Lake, Monticello, and Welsh plumes would increase to 7.0, 7.8, and 5.9, respectively, closing
10 roughly half of the gap between modeled and observed OPEs. For Big Brown, the OPE would
11 increase by a factor of 1.4, and for Parish, the OPE would increase to 6 (Pa^{-2}), exceeding the
12 observed OPE (4.4).

13

14 **5 Discussion and Conclusions**

15 A regional 3D photochemical model was applied with fine-grid resolution to simulate PPPs
16 during three days of airborne measurement by NOAA's WP-3 aircraft in TexAQS II. In
17 comprehensive evaluation of the model performance, the modeled and airborne observed
18 concentrations are compared in detail at each plume transect, which has rarely been done due to
19 the scarcity of the airborne observation of PPPs. Under steady wind meteorological conditions,
20 the fine-scale (4km) CMAQ demonstrated its ability to simulate the transport and dispersion of
21 PPPs despite lacking a plume-in-grid module.

1 SO₂ and NO_x show strong consistencies among the CEMS-reported emission data. In the
2 Martin Lake and Monticello plumes, CO was strongly correlated with SO₂ and NO_y and could
3 serve as a conservative tracer species to track plume evolution; CO₂ was strongly correlated with
4 SO₂ and NO_y in all plumes but was not modeled by CMAQ. The trend in the least square slopes
5 of pollutants relative to CO (CO₂) was used to assess species lifetime.

6 On clear-sky days (19 and 25 September), SO₂ and NO_y experienced slow evolution (loss) in
7 the Parish and Big Brown plumes. Both the model and the observation were closely correlated in
8 the ratios of SO₂ and NO_y to conservative species, suggesting the model well captured SO₂ and
9 NO_y evolution in the plumes.

10 SO₂ was observed to be rapidly lost in the Martin Lake, Monticello, and Welsh plumes under
11 scattered cloudiness on 16 September. The observation-based SO₂ lifetime was 2.6 and 2.7 hours
12 for the Martin Lake and Monticello plumes, respectively. The detailed examination of the
13 photolysis rate and relative humidity data suggested cloud-processing of PPPs caused the rapid
14 SO₂ loss on 16 September. The original simulation did not show the apparent SO₂ loss since
15 PPPs resided below clouds in the model. Perturbing the cloud bottom heights to interact with the
16 PPPs yielded modest rates of SO₂ removal via aqueous processing in the CMAQ cloud module.
17 SO₂ removal in the model was still slower than the observed rapid loss, even after increasing
18 cloud liquid water content and metals concentrations in cloud droplets to enhance SO₂ oxidation.

19 The simulation closely matched the observed NO_x oxidation rates. The observed NO_x
20 lifetime for Martin Lake and Monticello plumes was 2.6 hours and 1.2 hours, respectively. The
21 modeled PAN formation reflected the observed trend of PAN formation, while the modeled
22 HNO₃ was 0.7~6.6 times higher than observed due to the rapid HNO₃ loss in observation on
23 cloudy days. Martin Lake, Monticello, and Welsh plumes showed the similar extent of NO_y loss.

1 For the Martin Lake plume, the loss rate of NO_y has been quantified to be 0.148 hour^{-1} in
2 observation, faster than the modeled NO_y (0.026 hour^{-1}) by a factor of 6. In the model, NO_y loss
3 was insensitive to the aqueous processing when there was no precipitation happening. This
4 study, together with modeling studies, shows that the numerical representation of cloud aqueous
5 processing remains a major challenge.

6 The model effectively simulated the transition between ozone titration and formation but
7 tended to under-predict the magnitude of O_3 production and the OPE indicated by observations.
8 The discrepancies of OPEs between the model and the observations could be explained by the
9 observed rapid NO_y loss that biases high the observation-based OPE estimates, or under-
10 prediction of isoprene emissions that leads the model to under-predict OPE.

11

12 **Acknowledgments**

13 The work of W. Zhou and D. S. Cohan was funded by the Shell Center for Sustainability at
14 Rice University and National Science Foundation CAREER Award Grant 087386. We thank
15 Robert Griffin at Rice University for helpful discussions on data analyses. We thank Ken Aikin
16 and Harald Stark in the NOAA ESRL Chemical Sciences Division for help in using
17 meteorological and photolysis data. Although this article has been reviewed by the US EPA and
18 approved for publication, it does not necessarily reflect EPA policies or views.

19 **References**

- 20 Akimoto, H.: Global Air Quality and Pollution, *Science*, 302, 1716-1719,
21 10.1126/science.1092666, 2003.
- 22 Alexander, B., Park, R. J., Jacob, D. J., and Gong, S.: Transition metal-catalyzed oxidation of
23 atmospheric sulfur: Global implications for the sulfur budget, *J. Geophys. Res.*, 114, D02309,
24 10.1029/2008jd010486, 2009.

1 Appel, K. W., Roselle, S. J., Gilliam, R. C., and Pleim, J. E.: Sensitivity of the Community
2 Multiscale Air Quality (CMAQ) Model v4.7 results for the eastern United States to MM5 and
3 WRF meteorological drivers, *Geosci. Model Dev. Discuss.*, 2, 1081-1114, 2009.

4 Binkowski, F. S., and Roselle, S. J.: Models-3 Community Multiscale Air Quality (CMAQ)
5 model aerosol component 1. Model description, *J. Geophys. Res.*, 108, 4183,
6 10.1029/2001jd001409, 2003.

7 Brock, C. A., Washenfelder, R. A., Trainer, M., Ryerson, T. B., Wilson, J. C., Reeves, J. M.,
8 Huey, L. G., Holloway, J. S., Parrish, D. D., Hübler, G., and Fehsenfeld, F. C.: Particle growth in
9 the plumes of coal-fired power plants, *J. Geophys. Res. - Atmos.*, 107, 10.1029/2001jd001062,
10 2002.

11 Brock, C. A., Trainer, M., Ryerson, T. B., Neuman, J. A., Parrish, D. D., Holloway, J. S., Nicks,
12 D. K., Jr., Frost, G. J., Hübler, G., Fehsenfeld, F. C., Wilson, J. C., Reeves, J. M., Lafleur, B. G.,
13 Hilbert, H., Atlas, E. L., Donnelly, S. G., Schauffler, S. M., Stroud, V. R., and Wiedinmyer, C.:
14 Particle growth in urban and industrial plumes in Texas, *J. Geophys. Res. - Atmos.*, 108,
15 10.1029/2002jd002746, 2003.

16 Byun, D., and Schere, K. L.: Review of the Governing Equations, Computational Algorithms,
17 and Other Components of the Models-3 Community Multiscale Air Quality (CMAQ) Modeling
18 System, *Appl. Mech. Rev.*, 59, 27-50, 2006.

19 Chandler, A. S., Choularton, T. W., Dollard, G. J., Gay, M. J., Gallagher, M. W., Hill, T. A.,
20 Jones, B. M. R., Penkett, S. A., Tyler, B. J., and Bandy, B.: A field study of the oxidation of SO₂
21 in a cap cloud at Great Dun Fell, *Q. J. Roy. Meteor. Soc.*, 115, 397-420, 1989.

22 Colella, P., and Woodward, P. R.: The Piecewise Parabolic Method (PPM) for gas-dynamical
23 simulations, *Journal of Computational Physics*, 54, 174-201, 1984.

24 Crutzen, P. J., and Lawrence, M. G.: The Impact of Precipitation Scavenging on the Transport of
25 Trace Gases: A 3-Dimensional Model Sensitivity Study, *Journal of Atmospheric Chemistry*, 37,
26 81-112, 10.1023/a:1006322926426, 2000.

27 Daube, B. C., Boering, K. A., Andrews, A. E., and Wofsy, S. C.: A High-Precision Fast-
28 Response Airborne CO₂ Analyzer for In Situ Sampling from the Surface to the Middle
29 Stratosphere, *J. Atmos. Ocean. Tech.*, 19, 1532-1543, doi:10.1175/1520-0426, 2002.

30 Dudhia, J.: Numerical study of convection observed during the winter monsoon experiment
31 using a mesoscale two-dimensional model, *J. Atmos. Sci.*, 46, 3077-3107, 1989.

32 EPA: Sparse Matrix Operational Kernel Emission model version 2.4 User's Manual,
33 <http://www.smoke-model.org/version2/index.cfg>, (last access: October 2009), 2006., 2006.

34 EPA, U. S.: NO_x Budget Trading Program 2003 progress and compliance report, Rep. EPA-430-
35 R-04-010, Clean Air Markets Div., Off. of Air and Radiat., Washington, D. C. , 2004.

36 EPA, U. S.: Acid Rain Program 2002 progress report, Rep. EPA-430-R-03-011, Clean Air
37 Markets Div., Off. of Air and Radiat., Washington, D. C. , 2005.

38 Fang, Y., Fiore, A. M., Horowitz, L. W., Levy, H., II, Hu, Y., and Russell, A. G.: Sensitivity of
39 the NO_y budget over the United States to anthropogenic and lightning NO_x in summer, *J.*
40 *Geophys. Res.*, 115, D18312, 10.1029/2010jd014079, 2010.

1 Fiedler, V., Arnold, F., Schlager, H., Dörnbrack, A., Pirjola, L., and Stohl, A.: East Asian SO₂
2 pollution plume over Europe – Part 2: Evolution and potential impact, *Atmos. Chem.*
3 *Phys.*, 9, 4729-4745, 10.5194/acp-9-4729-2009, 2009.

4 Flues, M., Hama, P., Lemes, M. J. L., Dantas, E. S. K., and Fornaro, A.: Evaluation of the
5 rainwater acidity of a rural region due to a coal-fired power plant in Brazil, *Atmos. Environ.*, 36,
6 2397-2404, 2002.

7 Foley, K. M., Roselle, S. J., Appel, K. W., Bhave, P. V., Pleim, J. E., Otte, T. L., Mathur, R.,
8 Sarwar, G., Young, J. O., Gilliam, R. C., Nolte, C. G., Kelly, J. T., Gilliland, A. B., and Bash, J.
9 O.: Incremental testing of the Community Multiscale Air Quality (CMAQ) modeling system
10 version 4.7, *Geosci. Model Dev.*, 3, 205-226, 10.5194/gmd-3-205-2010, 2010.

11 Kreidenweis, S. M., Zhang, Y., and Taylor, G. R.: The effects of clouds on aerosol and chemical
12 species production and distribution 2. Chemistry model description and sensitivity analysis, *J.*
13 *Geophys. Res.*, 102, 23867-23882, 10.1029/97jd00775, 1997.

14 Frost, G. J., McKeen, S. A., Trainer, M., Ryerson, T. B., Neuman, J. A., Roberts, J. M.,
15 Swanson, A., Holloway, J. S., Sueper, D. T., Fortin, T., Parrish, D. D., Fehsenfeld, F. C., Flocke,
16 F., Peckham, S. E., Grell, G. A., Kowal, D., Cartwright, J., Auerbach, N., and Habermann, T.:
17 Effects of changing power plant NO_x emissions on ozone in the eastern United States: Proof of
18 concept, *J. Geophys. Res. - Atmos.*, 111, 10.1029/2005jd006354, 2006.

19 Godowitch, J. M., Gilliland, A. B., Draxler, R. R., and Rao, S. T.: Modeling assessment of point
20 source NO_x emission reductions on ozone air quality in the eastern United States, *Atmos.*
21 *Environ.*, 42, 87-100, 2008.

22 Godowitch, Hogrefe, C., and Rao, S. T.: Diagnostic analyses of a regional air quality model:
23 Changes in modeled processes affecting ozone and chemical-transport indicators from NO_x
24 point source emission reductions, *J. Geophys. Res. - Atmos.*, 113, 10.1029/2007jd009537, 2008.

25 Grell, G. A., Dudhia, J., and Stauffer, D. R.: A description of the Fifth-Generation Penn
26 State/NCAR Mesoscale Model (MM5). NCAR Technical Note NCAR/TN-398+STR, 1994.

27 Griffin, R. J., Johnson, C. A., Talbot, R. W., Mao, H., Russo, R. S., Zhou, Y., and Sive, B. C.:
28 Quantification of ozone formation metrics at Thompson Farm during the New England Air
29 Quality Study (NEAQS) 2002, *J. Geophys. Res. - Atmos.*, 109, D24302, 10.1029/2004jd005344,
30 2004.

31 Guenther, A., Geron, C., Pierce, T., Lamb, B., Harley, P., and Fall, R.: Natural emissions of non-
32 methane volatile organic compounds, carbon monoxide, and oxides of nitrogen from North
33 America, *Atmos. Environ.*, 34, 2205-2230, 2000.

34 Hudman, R. C., Murray, L. T., Jacob, D. J., Turquety, S., Wu, S., Millet, D. B., Avery, M.,
35 Goldstein, A. H., and Holloway, J.: North American influence on tropospheric ozone and the
36 effects of recent emission reductions: Constraints from ICARTT observations, *J. Geophys. Res. -*
37 *Atmos.*, 114, 10.1029/2008jd010126, 2009.

38 Jayne, J. T., Leard, D. C., Zhang, X., Davidovits, P., Smith, K. A., Kolb, C. E., and Worsnop, D.
39 R.: Development of an Aerosol Mass Spectrometer for Size and Composition Analysis of
40 Submicron Particles, *Aerosol Science and Technology*, 33, 49 - 70, 2000.

1 Kain, J. S.: The Kain-Fritsch convective parameterization: An update, *J. Appl. Meteorol*, 43,
2 170-181, 2004.

3 Karamchandani, P., Koo, A., and Seigneur, C.: Reduced Gas-Phase Kinetic Mechanism for
4 Atmospheric Plume Chemistry, *Environ. Sci. Technol*, 32, 1709-1720, 10.1021/es970707u,
5 1998.

6 Karamchandani, P., Santos, L., Sykes, I., Zhang, Y., Tonne, C., and Seigneur, C.: Development
7 and Evaluation of a State-of-the-Science Reactive Plume Model, *Environ. Sci. Technol*, 34, 870-
8 880, 10.1021/es990611v, 2000.

9 Karamchandani, P., Seigneur, C., Vijayaraghavan, K., and Wu, S.-Y.: Development and
10 application of a state-of-the-science plume-in-grid model, *J. Geophys. Res. - Atmos.*, 107,
11 10.1029/2002jd002123, 2002.

12 Kim, S. W., Heckel, A., McKeen, S. A., Frost, G. J., Hsie, E. Y., Trainer, M. K., Richter, A.,
13 Burrows, J. P., Peckham, S. E., and Grell, G. A.: Satellite-observed U.S. power plant NOx
14 emission reductions and their impact on air quality, *Geophys. Res. Lett.*, 33,
15 10.1029/2006gl027749, 2006.

16 Kleinman, L. I., Daum, P. H., Lee, Y.-N., Nunnermacker, L. J., Springston, S. R., Weinstein-
17 Lloyd, J., and Rudolph, J.: Ozone production efficiency in an urban area, *J. Geophys. Res. -
18 Atmos.*, 107, 4733, 10.1029/2002jd002529, 2002.

19 Lee, C., Martin, R. V., van Donkelaar, A., Lee, H., Dickerson, R. R., Hains, J. C., Krotkov, N.,
20 Richter, A., Vinnikov, K., and Schwab, J. J.: SO₂ emissions and lifetimes: Estimates from
21 inverse modeling using in situ and global, space-based (SCIAMACHY and OMI) observations,
22 *J. Geophys. Res.*, 116, D06304, 10.1029/2010jd014758, 2011.

23 Liu, S. C., Trainer, M., Fehsenfeld, F. C., Parrish, D. D., Williams, E. J., Fahey, D. W., Hübler,
24 G., and Murphy, P. C.: Ozone Production in the Rural Troposphere and the Implications for
25 Regional and Global Ozone Distributions, *J. Geophys. Res. - Atmos.*, 92, 4191-4207,
26 10.1029/JD092iD04p04191, 1987.

27 Luria, M., Imhoff, R., Valente, R., Parkhurst, W., and Tanner, R.: Rates of conversion of sulfur
28 dioxide to sulfate in a scrubbed power plant plume, *J. Air Waste Manage. Assoc.*, 51, 1408-1413
29 2001.

30 Mauzerall, D. L., Sultan, B., Kim, N., and Bradford, D. F.: NO_x emissions from large point
31 sources: variability in ozone production, resulting health damages and economic costs, *Atmos.
32 Environ.*, 39, 2851-2866, 2005.

33 Meng, Z., and Seinfeld, J. H.: On the Source of the Submicrometer Droplet Mode of Urban and
34 Regional Aerosols, *Aerosol. Sci. Tech.*, 20, 253 - 265, 1994.

35 Mlawer, E. J., Taubman, S. J., Brown, P. D., Iacono, M. J., and Clough, S. A.: Radiative transfer
36 for inhomogeneous atmospheres: RRTM, a validated correlated-k model for the longwave, *J.
37 Geophys. Res. - Atmos.*, 102, 16663-16682, 1997.

38 Neuman, J. A., Parrish, D. D., Ryerson, T. B., Brock, C. A., Wiedinmyer, C., Frost, G. J.,
39 Holloway, J. S., and Fehsenfeld, F. C.: Nitric acid loss rates measured in power plant plumes, *J.
40 Geophys. Res. - Atmos.*, 109, 10.1029/2004jd005092, 2004.

1 Neuman, J. A., Parrish, D. D., Trainer, M., Ryerson, T. B., Holloway, J. S., Nowak, J. B.,
2 Swanson, A., Flocke, F., Roberts, J. M., Brown, S. S., Stark, H., Sommariva, R., Stohl, A.,
3 Peltier, R., Weber, R., Wollny, A. G., Sueper, D. T., Hubler, G., and Fehsenfeld, F. C.: Reactive
4 nitrogen transport and photochemistry in urban plumes over the North Atlantic Ocean, *J.*
5 *Geophys. Res. - Atmos.*, 111, 10.1029/2005jd007010, 2006.

6 Neuman, J. A., Nowak, J. B., Zheng, W., Flocke, F., Ryerson, T. B., Trainer, M., Holloway, J.
7 S., Parrish, D. D., Frost, G. J., Peischl, J., Atlas, E. L., Bahreini, R., Wollny, A. G., and
8 Fehsenfeld, F. C.: Relationship between photochemical ozone production and NO_x oxidation in
9 Houston, Texas, *J. Geophys. Res. - Atmos.*, 114, 10.1029/2008jd011688, 2009.

10 Nicks, D. K., Holloway, J. S., Ryerson, T. B., Dissly, R. W., Parrish, D. D., Frost, G. J., Trainer,
11 M., Donnelly, S. G., Schauffler, S., Atlas, E. L., Hubler, G., Sueper, D. T., and Fehsenfeld, F. C.:
12 Fossil-fueled power plants as a source of atmospheric carbon monoxide, *J. Environ. Monitor.*, 5,
13 35-39, 2003.

14 Nowak, J. B., Neuman, J. A., Bahreini, R., Brock, C. A., Middlebrook, A. M., Wollny, A. G.,
15 Holloway, J. S., Peischl, J., Ryerson, T. B., and Fehsenfeld, F. C.: Airborne observations of
16 ammonia and ammonium nitrate formation over Houston, Texas, *J. Geophys. Res. - Atmos.*, In
17 press, 2010.

18 Nunnermacker, L. J., Kleinman, L. I., Imre, D., Daum, P. H., Lee, Y. N., Lee, J. H., Springston,
19 S. R., Newman, L., and Gillani, N.: NO_y lifetimes and O₃ production efficiencies in urban and
20 power plant plumes: Analysis of field data, *J. Geophys. Res. - Atmos.*, 105, 9165-9176,
21 10.1029/1999jd900753, 2000.

22 Oppenheimer, C., Kyle, P., Eisele, F., Crawford, J., Huey, G., Tanner, D., Kim, S., Mauldin, L.,
23 Blake, D., Beyersdorf, A., Buhr, M., and Davis, D.: Atmospheric chemistry of an Antarctic
24 volcanic plume, *J. Geophys. Res. - Atmos.*, 115, D04303, 10.1029/2009jd011910, 2010.

25 Otte, T. L., and Pleim, J. E.: The Meteorology-Chemistry Interface Processor (MCIP) for the
26 CMAQ modeling system, *Geosci. Model Dev. Discuss.*, 2, 1449-1486, 2009.

27 Parazols, M., Marinoni, A., Amato, P., Abida, O., Laj, P., and Mailhot, G.: Speciation and role of
28 iron in cloud droplets at the puy de Dôme station, *Journal of Atmospheric Chemistry*, 54, 267-
29 281, 10.1007/s10874-006-9026-x, 2006.

30 Parrish, D. D., Allen, D. T., Bates, T. S., Estes, M., Fehsenfeld, F. C., Feingold, G., Ferrare, R.,
31 Hardesty, R. M., Meagher, J. F., Nielsen-Gammon, J. W., Pierce, R. B., Ryerson, T. B., Seinfeld,
32 J. H., and Williams, E. J.: Overview of the Second Texas Air Quality Study (TexAQS II) and the
33 Gulf of Mexico Atmospheric Composition and Climate Study (GoMACCS), *J. Geophys. Res. -*
34 *Atmos.*, 114, 10.1029/2009jd011842, 2009a.

35 Parrish, D. D., Millet, D. B., and Goldstein, A. H.: Increasing ozone in marine boundary layer
36 inflow at the west coasts of North America and Europe, *Atmos. Chem. Phys.*, 9, 1303-1323,
37 2009b.

38 Peischl, J., Ryerson, T. B., Holloway, J. S., Parrish, D. D., Trainer, M., Frost, G. J., Aikin, K. C.,
39 Brown, S. S., Dubé, W. P., Stark, H., and Fehsenfeld, F. C.: A top-down analysis of emissions
40 from selected Texas power plants during TexAQS 2000 and 2006, *J. Geophys. Res. - Atmos.*,
41 115, D16303, 10.1029/2009jd013527, 2010.

1 Pleim, J. E.: A Combined Local and Nonlocal Closure Model for the Atmospheric Boundary
2 Layer. Part I: Model Description and Testing, *J. Appl. Meteorol. Clim*, 46, 1383-1395,
3 doi:10.1175/JAM2539.1, 2007.

4 Raja, S., Ravikrishna, R., Kommalapati, R., and Valsaraj, K.: Monitoring of Fogwater Chemistry
5 in the Gulf Coast Urban Industrial Corridor: Baton Rouge (Louisiana), *Environmental*
6 *Monitoring and Assessment*, 110, 99-120, 10.1007/s10661-005-6281-2, 2005.

7 Rodríguez, L. A., Watson, I. M., Edmonds, M., Ryan, G., Hards, V., Oppenheimer, C. M. M.,
8 and Bluth, G. J. S.: SO₂ loss rates in the plume emitted by Soufrière Hills volcano, Montserrat, *J.*
9 *Volcanol. Geoth. Res.*, 173, 135-147, 2008.

10 Ryerson, T. B., Buhr, M. P., Frost, G. J., Goldan, P. D., Holloway, J. S., Hübler, G., Jobson, B.
11 T., Kuster, W. C., McKeen, S. A., Parrish, D. D., Roberts, J. M., Sueper, D. T., Trainer, M.,
12 Williams, J., and Fehsenfeld, F. C.: Emissions lifetimes and ozone formation in power plant
13 plumes, *J. Geophys. Res. - Atmos.*, 103, 10.1029/98jd01620, 1998.

14 Ryerson, T. B., Trainer, M., Holloway, J. S., Parrish, D. D., Huey, L. G., Sueper, D. T., Frost, G.
15 J., Donnelly, S. G., Schauffler, S., Atlas, E. L., Kuster, W. C., Goldan, P. D., Hubler, G.,
16 Meagher, J. F., and Fehsenfeld, F. C.: Observations of Ozone Formation in Power Plant Plumes
17 and Implications for Ozone Control Strategies, *Science*, 292, 719-723, 10.1126/science.1058113,
18 2001.

19 Ryerson, T. B., Trainer, M., Angevine, W. M., Brock, C. A., Dissly, R. W., Fehsenfeld, F. C.,
20 Frost, G. J., Goldan, P. D., Holloway, J. S., Hübler, G., Jakoubek, R. O., Kuster, W. C., Neuman,
21 J. A., Nicks, D. K., Jr., Parrish, D. D., Roberts, J. M., Sueper, D. T., Atlas, E. L., Donnelly, S. G.,
22 Flocke, F., Fried, A., Potter, W. T., Schauffler, S., Stroud, V., Weinheimer, A. J., Wert, B. P.,
23 Wiedinmyer, C., Alvarez, R. J., Banta, R. M., Darby, L. S., and Senff, C. J.: Effect of
24 petrochemical industrial emissions of reactive alkenes and NO_x on tropospheric ozone formation
25 in Houston, Texas, *J. Geophys. Res. - Atmos.*, 108, 10.1029/2002jd003070, 2003.

26 Schwartz, S. E.: Mass-transport limitation to the rate of in-cloud oxidation of SO₂: Re-
27 examination in the light of new data, *Atmos. Environ.*, 22, 2491-2499, 1988.

28 Sillman, S., Logan, J. A., and Wofsy, S. C.: A Regional Scale Model for Ozone in the United
29 States With Subgrid Representation of Urban and Power Plant Plumes, *J. Geophys. Res.*, 95,
30 10.1029/JD095iD05p05731, 1990.

31 Sillman, S.: Ozone production efficiency and loss of NO_x in power plant plumes: Photochemical
32 model and interpretation of measurements in Tennessee, *J. Geophys. Res. - Atmos.*, 105,
33 10.1029/1999jd901014, 2000.

34 Skamarock, W. C., Klemp, J. B., Dudhia, J., Gill, D., Barker, D. M., Duda, M. G., Huang, X.-Y.,
35 Ang, W., and Powers, J. G.: A description of the advanced research WRF version 3. NCAR
36 Technical Note NCAR/TN 475 STR, 2008.

37 Springston, S. R., Kleinman, L. I., Brechtel, F., Lee, Y.-N., Nunnermacker, L. J., and Wang, J.:
38 Chemical evolution of an isolated power plant plume during the TexAQS 2000 study, *Atmos.*
39 *Environ.*, 39, 3431-3443, 2005.

40 Srivastava, R. K., Miller, C. A., Erickson, C., and Jambhekar, R.: Emissions of sulfur trioxide
41 from coal-fired power plants, *J. Air Waste Manage. Assoc.*, 54, 750-762, 2004.

1 Takegawa, N., Kondo, Y., Koike, M., Ko, M., Kita, K., Blake, D. R., Nishi, N., Hu, W., Liley, J.
2 B., Kawakami, S., Shirai, T., Miyazaki, Y., Ikeda, H., Russel-Smith, J., and Ogawa, T.: Removal
3 of NO_x and NO_y in biomass burning plumes in the boundary layer over northern Australia, *J.*
4 *Geophys. Res. - Atmos.*, 108, 4308, 10.1029/2002jd002505, 2003.

5 Thompson, G., Rasmussen, R. M., and Manning, K.: Explicit Forecasts of Winter Precipitation
6 Using an Improved Bulk Microphysics Scheme. Part I: Description and Sensitivity Analysis,
7 *Mon. Weather. Rev.*, 132, 519-542, doi:10.1175/1520-0493, 2004.

8 Trainer, M., Parrish, D. D., Buhr, M. P., Norton, R. B., Fehsenfeld, F. C., Anlauf, K. G.,
9 Bottenheim, J. W., Tang, Y. Z., Wiebe, H. A., Roberts, J. M., Tanner, R. L., Newman, L.,
10 Bowersox, V. C., Meagher, J. F., Olszyna, K. J., Rodgers, M. O., Wang, T., Berresheim, H.,
11 Demerjian, K. L., and Roychowdhury, U. K.: Correlation of ozone with NO_y in photochemically
12 aged air, *J. Geophys. Res. - Atmos.*, 98, 2917-2925, 10.1029/92jd01910, 1993.

13 Trainer, M., Ridley, B. A., Buhr, M. P., Kok, G., Walega, J., Hübler, G., Parrish, D. D., and
14 Fehsenfeld, F. C.: Regional ozone and urban plumes in the southeastern United States:
15 Birmingham, a case study, *J. Geophys. Res. - Atmos.*, 100, 18823-18834, 10.1029/95jd01641,
16 1995.

17 Vijayaraghavan, K., Karamchandani, P., and Seigneur, C.: Plume-in-grid modeling of summer
18 air pollution in Central California, *Atmos. Environ.*, 40, 5097-5109, 2006.

19 Vijayaraghavan, K., Zhang, Y., Seigneur, C., Karamchandani, P., and Snell, H. E.: Export of
20 reactive nitrogen from coal-fired power plants in the U.S.: Estimates from a plume-in-grid
21 modeling study, *J. Geophys. Res. - Atmos.*, 114, 10.1029/2008jd010432, 2009.

22 Walcek, C. J., and Taylor, G. R.: A Theoretical Method for Computing Vertical Distributions of
23 Acidity and Sulfate Production within Cumulus Clouds, *J. Atmos. Sci.*, 43, 339-355,
24 doi:10.1175/1520-0469(1986)043<0339:ATMFCV>2.0.CO;2, 1986.

25 Xiu, A., and Pleim, J. E.: Development of a Land Surface Model. Part I: Application in a
26 Mesoscale Meteorological Model, *J. Appl. Meteorol*, 40, 192-209, doi:10.1175/1520-
27 0450(2001), 2001.

28 Yarwood, G., Rao, S., Yocke, M., and Whitten, G.: Updates to the Carbon Bond Chemical
29 Mechanism: CB05 Final Report to the US EPA, RT-0400675, 2005.

30 Yu, S., Mathur, R., Sarwar, G., Kang, D., Tong, D., Pouliot, G., and Pleim, J.: Eta-CMAQ air
31 quality forecasts for O₃ and related species using three different photochemical mechanisms
32 (CB4, CB05, SAPRC-99): comparisons with measurements during the 2004 ICARTT study,
33 *Atmos. Chem. Phys.*, 10, 3001-3025, 10.5194/acp-10-3001-2010, 2010.

34 Yamartino, R. J.: Nonnegative, Conserved Scalar Transport Using Grid-Cell-centered, Spectrally
35 Constrained Blackman Cubics for Applications on a Variable-Thickness Mesh, *Monthly*
36 *Weather Review*, 121, 753-763, doi:10.1175/1520-0493(1993)121<0753:NCSTUG>2.0.CO;2,
37 1993.

38 Zaveri, R. A., Berkowitz, C. M., Kleinman, L. I., Springston, S. R., Doskey, P. V., Lonneman,
39 W. A., and Spicer, C. W.: Ozone production efficiency and NO_x depletion in an urban plume:
40 Interpretation of field observations and implications for evaluating O₃-NO_x-VOC sensitivity, *J.*
41 *Geophys. Res.*, 108, 4436, 10.1029/2002jd003144, 2003.

42

1 Table 1. Major power plants in eastern Texas

Facility	NO _x emission rate ^a (tons/hour)	SO ₂ emission rate ^a (tons/hour)	Stack Height (m)
Martin Lake	2.02	10.37	138
Monticello	1.34	5.49	128
Welsh	0.95	2.21	172
Pirkey	0.58	0.21	160
Big Brown	0.84	13.09	122
Parish	0.33	2.74	183
Limestone	0.79	0.63	137

2 ^a emission rate is the hourly averaged CEMS data for Martin Lake, Monticello, and Welsh on 16
 3 September, 2006, and for Parish, Big Brown, and Limestone on 25 September, 2006.

4
5
6
7
8
9
10
11
12
13
14
15
16
17

1 Table 2. CEMS-reported E(SO₂)/E(NO_x) emission molar ratio, the observed SO₂/NO_y and the
 2 modeled ZOC_{SO₂}/ZOC_{NO_y} at the location of the first plume transect.

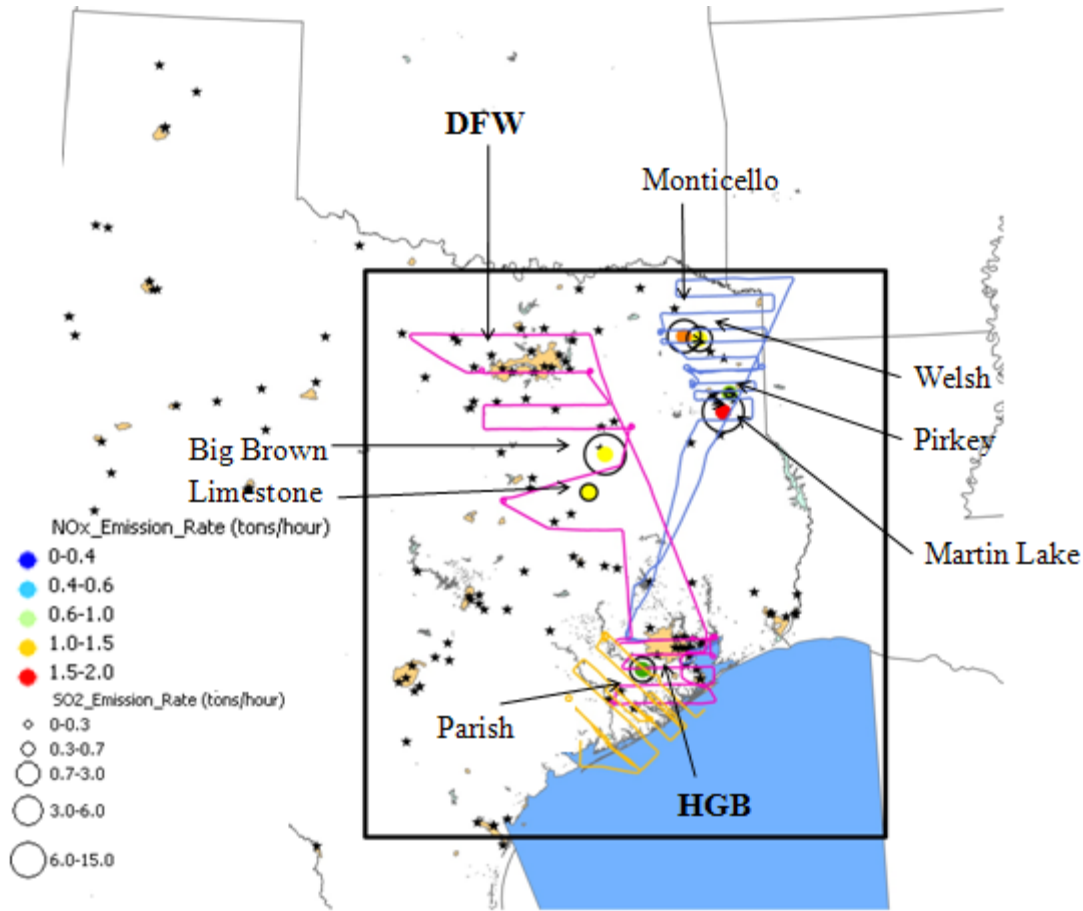
Plant	CEMS SO ₂ /NO _x	OBS SO ₂ /NO _y ^a	MODEL ZOC _{SO₂} /ZOC _{NO_y} ^b	Plume age (hours)
Martin Lake	3.05	3.94 (0.98)	3.30	0.7
Monticello	2.04	3.00 (0.86)	1.84	0.3
Welsh	1.10	1.20 (0.86)	1.08	0.4
Big Brown	8.94	10.95 (0.97)	9.73	1.3
Parish	5.28	6.83 (0.68)	5.18	0.6

3 ^a the values in brackets are the R² of least square fit of SO₂ versus NO_y

4 ^b ZOC_{SO₂} = SO₂ model, base - SO₂ model, zero-out that plant, ZOC_{NO_y} = NO_y model, base - NO_y model, zero-out that
 5 plant

6
7
8
9
10
11
12
13
14
15
16
17
18
19
20

1



2

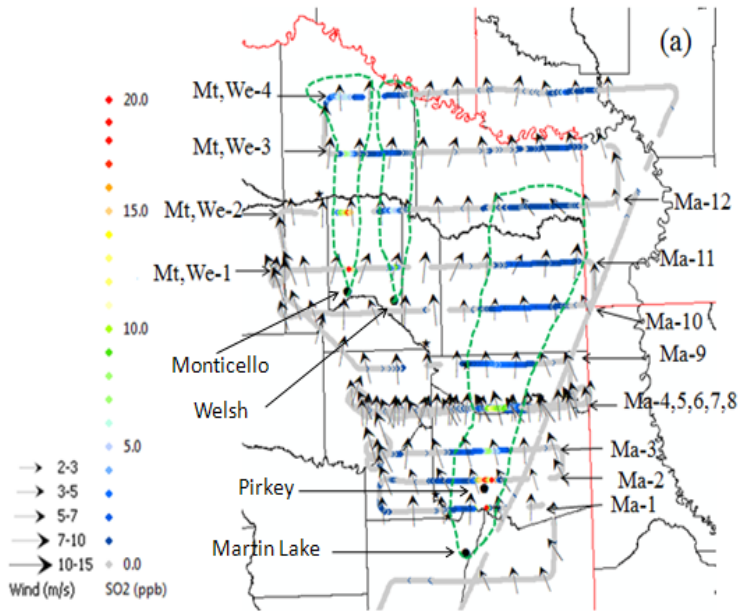
3 Fig. 1. WP-3 flight tracks (16 September in blue, 19 September in yellow, and 25 September in
4 pink,) and power plants in eastern Texas. NO_x emission rates are shown by colors and SO₂
5 emission rates are indicated by size of circles. Rectangular frame shows the 4km modeling
6 domain. Black stars are all other point sources in Texas. The Houston-Galveston-Brazoria
7 (HGB) and Dallas-Forth-Worth (DFW) metropolitan areas are also shown.

8

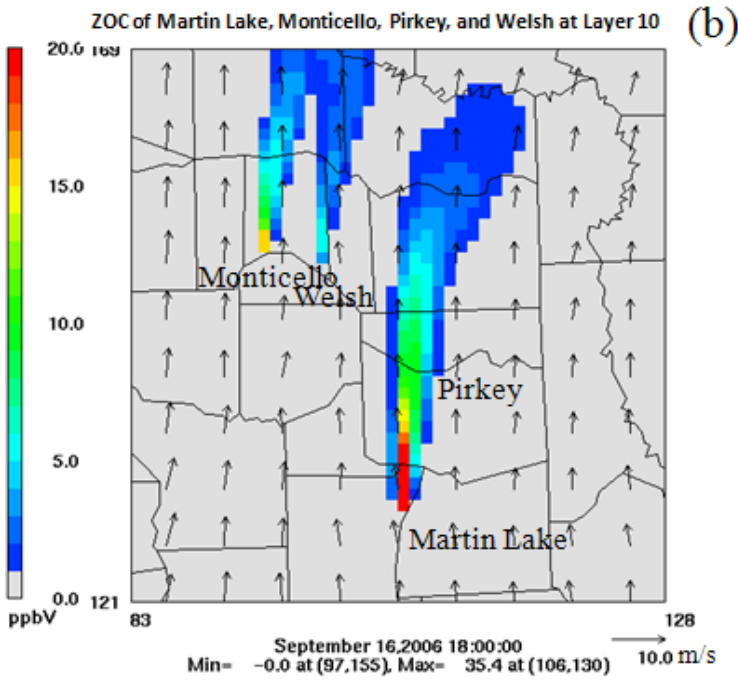
9

10

11

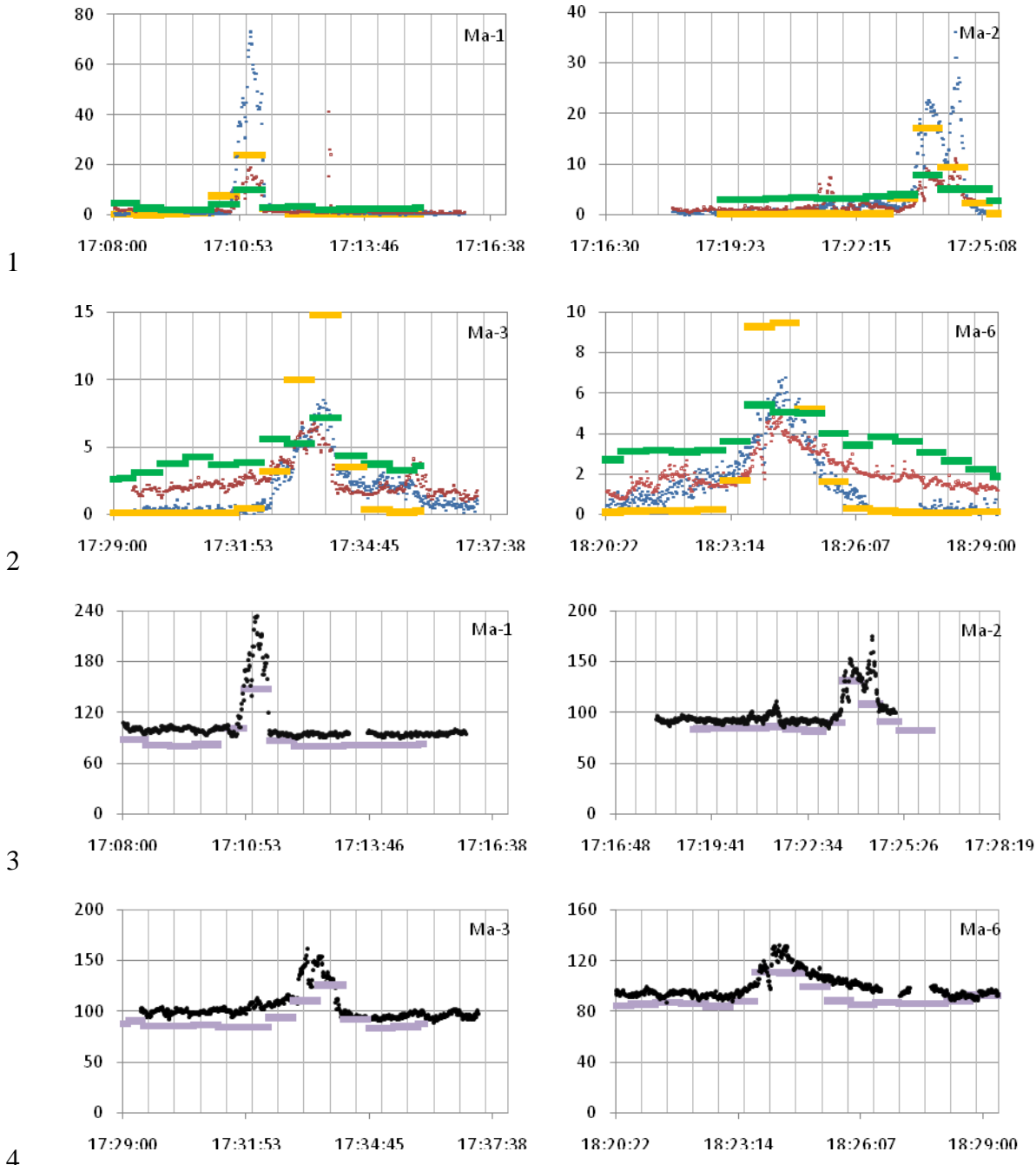


1

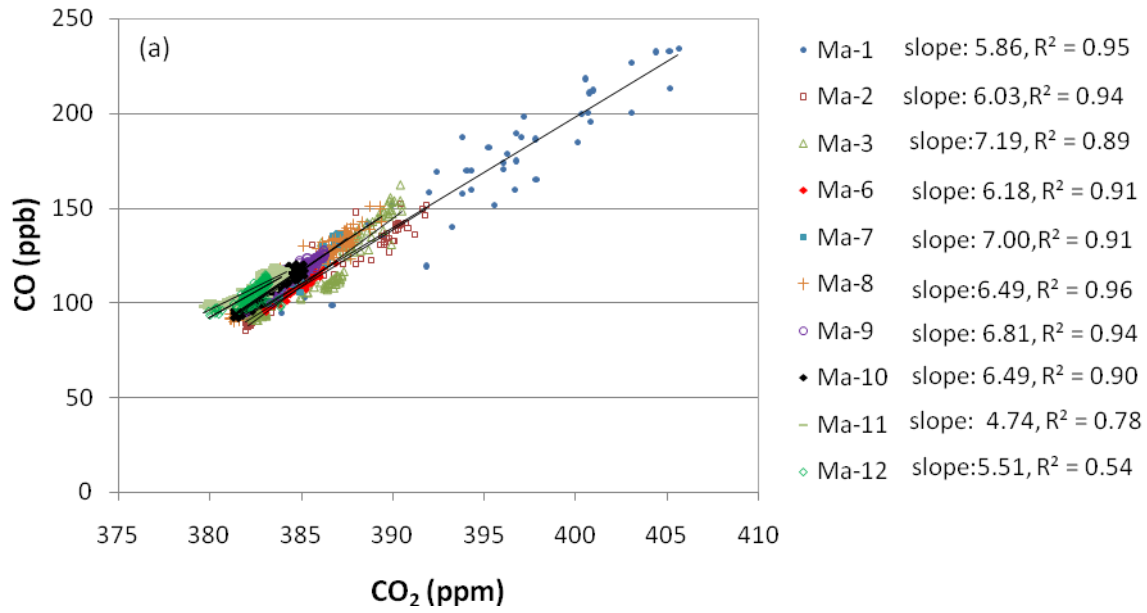


2

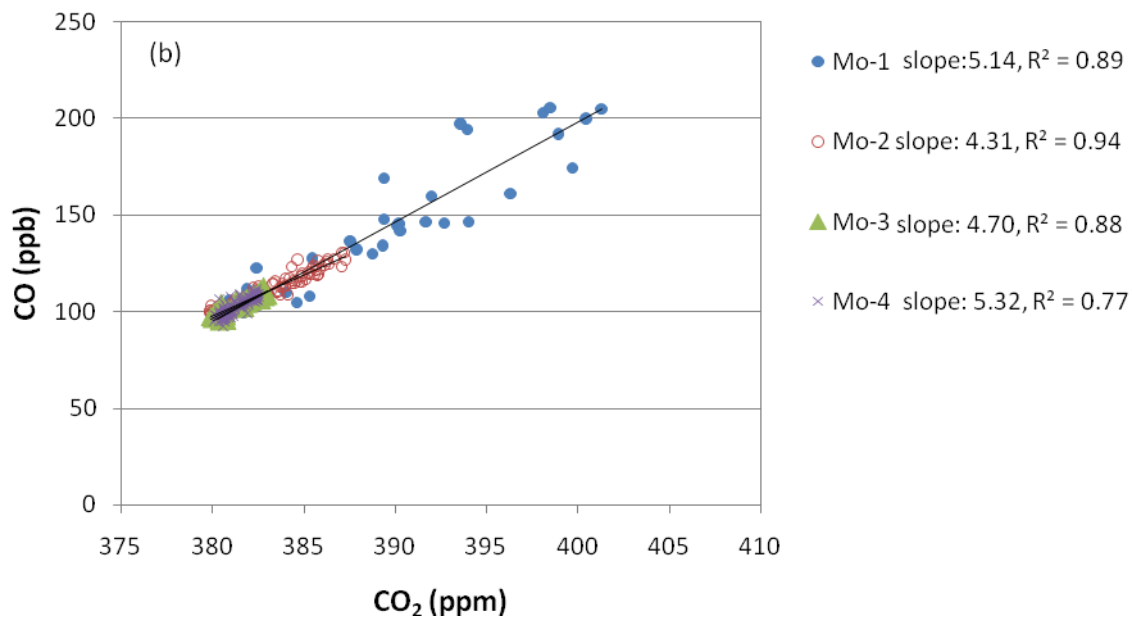
3 Fig. 2. (a) Observed PPPs of Martin Lake, Monticello, Pirkey, and Welsh on 16 September,
 4 2006. The black dots show the locations of the power plants. PPPs are identified by measured
 5 SO₂ enhancement (color gradient in the figure), as outlined by the green dash lines. Measured
 6 wind vectors are presented on the plume transect. (b) Simulated PPPs of Martin Lake,
 7 Monticello, Pirkey, and Welsh at 18:00 GMT (600~700 m) (local time: 12:00)



5 Fig. 3. The comparison of the modeled and observed SO₂, NO_y, and CO at plume transect of
 6 Ma-1, Ma-2, Ma-3 and Ma-6. The modeled SO₂, NO_y, and CO are labeled as yellow, green, and
 7 purple flat lines, respectively. The observed SO₂, NO_y, and CO are labeled as blue, red and black
 8 dots. The Horizontal coordinate is time scale in GMT (local time = GMT - 6 hours) and vertical
 9 coordinate is concentration (ppb). Transect names listed in Table S3 of the manuscript are labeled
 10 in each subplot. Fig. S1-S4 summarize the comparisons for all the plume transects



1



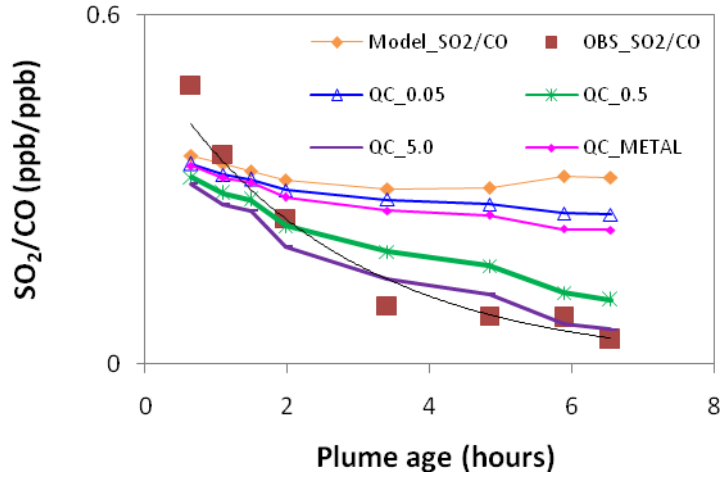
2

3 Fig. 4. Scatter plot of CO (ppb) versus CO₂ (ppm) from plume transects (a) Martin Lake (Ma-1
 4 to Ma-12), and (b) Monticello (Mo-1 to Mo-4). The unit of the slopes from the least square fits is
 5 ppb/ppm.

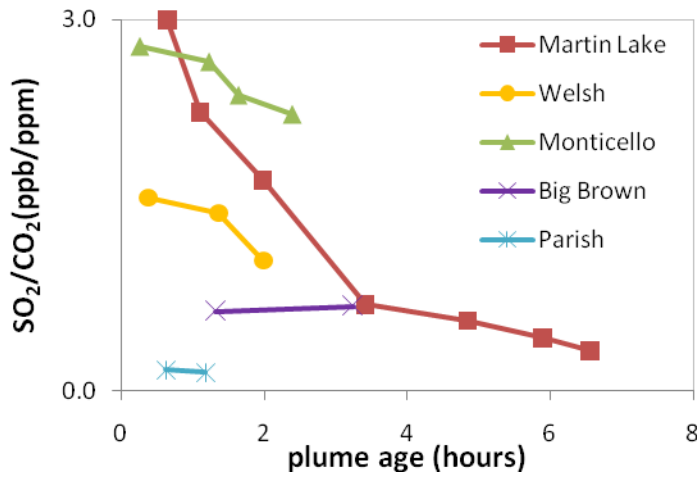
6

7

8



1



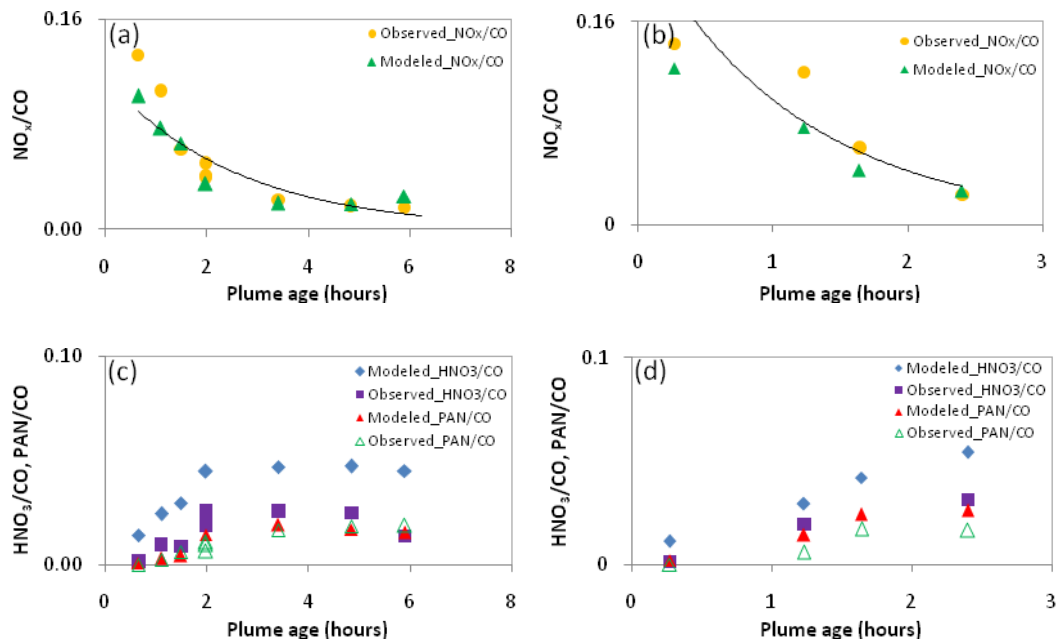
2

3 Fig. 5. (a) The observed least square slopes of SO_2 to CO (red square) and modeled
 4 $\text{ZOC}_{\text{SO}_2}/\text{ZOC}_{\text{CO}}$ (blue diamond for the base case, green dot for the adjusted cloud case) as a
 5 function of plume age at each transect of the Martin Lake plume (16 September). The observed
 6 SO_2 loss rate was 0.38 hour^{-1} ($R^2=0.94$, SO_2 lifetime: 2.6 hours); the modeled SO_2 loss rate was
 7 0.016 hour^{-1} ($R^2=0.36$, SO_2 lifetime: 62.5 hours). The SO_2 to CO slopes for each perturbation
 8 case are also plotted accordingly. (b) The observed least square slopes of SO_2 to CO_2 (ppb/ppm)
 9 for the five plumes; Martin Lake, Welsh, and Monticello plumes were observed on September 16
 10 (cloudy day), Big Brown and Parish plumes were made on 25 September (sunny day).

11

12

13



1

2

3 Fig. 6. Observed (yellow circle) and modeled (green triangle) NO_x/CO (a) for the Martin Lake
 4 plume, (b) for the Monticello plume. The observed NO_x oxidation rate was 0.38 hour^{-1} ($R^2=0.85$)
 5 for the Martin Lake plume and 0.84 hour^{-1} ($R^2=0.86$) for the Monticello plume. Observed and
 6 modeled PAN/CO and HNO_3/CO , (c) for the Martin Lake plume, (d) for the Monticello plume.

7

8

9

10

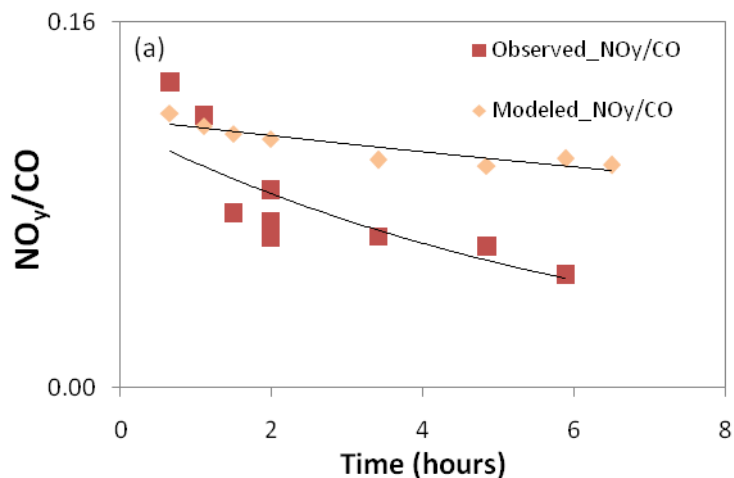
11

12

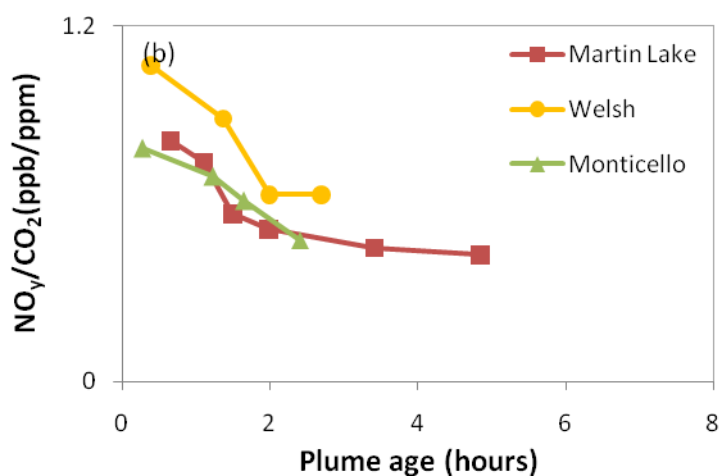
13

14

15



1



2

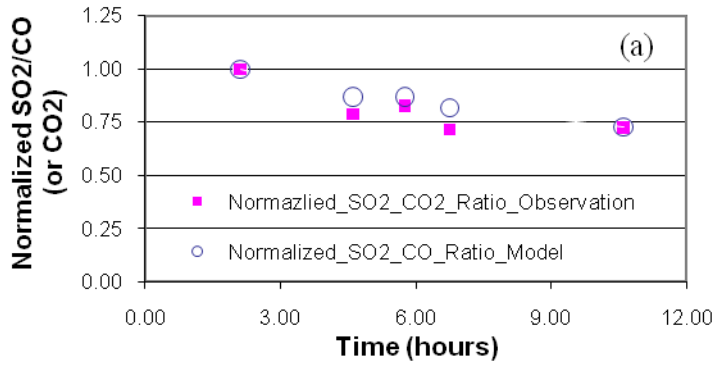
3 Fig. 7. (a) The observed least square slopes of NO_y to CO (red square) and modeled
 4 $\text{ZOC}_{\text{NO}_y}/\text{ZOC}_{\text{CO}}$ (orange diamond for the base case, green dot for the adjusted cloud case) as a
 5 function of plume age at each transect of the Martin Lake plume; the observed NO_y loss rate was
 6 0.145 hour^{-1} ($R^2=0.69$) and the modeled NO_y loss rate was 0.026 hour^{-1} ($R^2=0.48$). (b) The
 7 observed least square slopes of NO_y to CO_2 (ppb/ppm) for the Martin Lake, Monticello, and
 8 Welsh. NO_y in the least-square fits was directly measured and not the sum of measured reactive
 9 nitrogen species.

10

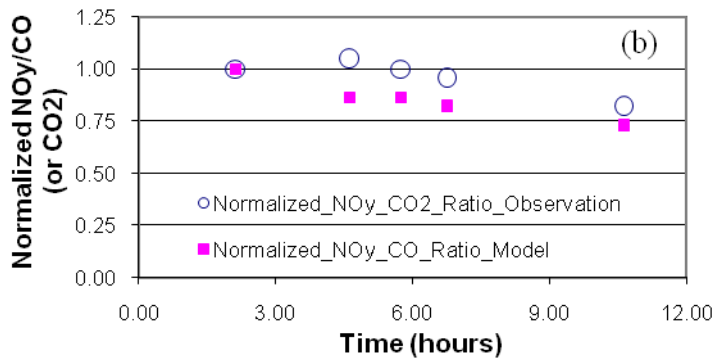
11

12

13



1



2

3 Fig. 8. The least-square-fit slopes of SO₂ to CO₂ (from the observation) and SO₂ to CO (from
 4 the model) (a), and the least-square-fit slopes of NO_y to CO₂ (from the observation) and NO_y to
 5 CO (from the observation) (b). All slopes are normalized to the slope at the first transect.

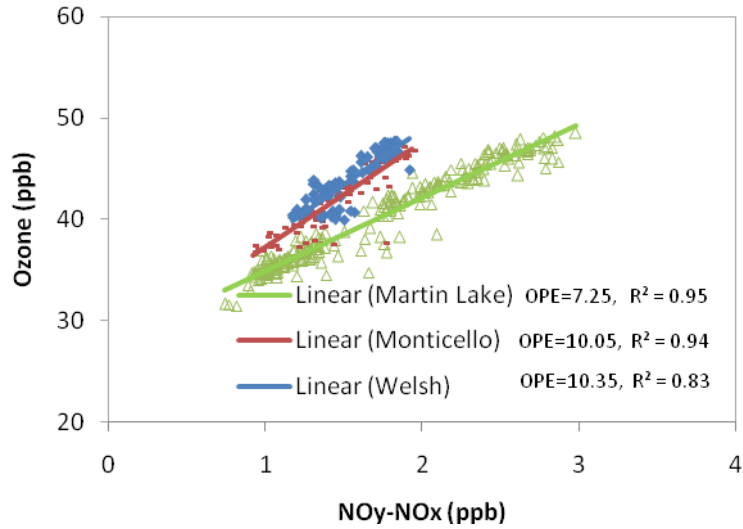
6

7

8

9

10



1
 2 Fig. 9. O₃ versus NO_y-NO_x from the transects of Martin Lake (Ma-6, plume age of 2.0 hours),
 3 Monticello (Mo-4, plume age of 2.4 hours), and Welsh (We-4, plume age of 2.7 hours). The
 4 slopes from the least square fits indicate the observation-based estimates of OPE from each
 5 plume transect.